The Plant Cell, Vol. 25: 1573–1591, May 2013, www.plantcell.org

oiwa, a Female Gametophytic Mutant Impaired in a Mitochondrial Manganese-Superoxide Dismutase, Reveals Crucial Roles for Reactive Oxygen Species during Embryo Sac Development and Fertilization in *Arabidopsis*[C][W]

María Victoria Martin,[a] Diego Fernando Fiol,[a] Venkatesan Sundaresan,[b,c] Eduardo Julián Zabaleta,[a] and Gabriela Carolina Pagnussat[a,1]

[a] Instituto de Investigaciones Biológicas IIB-Consejo Nacional de Investigaciones Científicas y Técnicas, Universidad Nacional de Mar del Plata, 7600 Mar del Plata, Argentina

[b] Department of Plant Biology, University of California, Davis, California 95616

[c] Department of Plant Sciences, University of California, Davis, California 95616

Reactive oxygen species (ROS) can function as signaling molecules, regulating key aspects of plant development, or as toxic compounds leading to oxidative damage. In this article, we show that the regulation of ROS production during megagametogenesis is largely dependent on MSD1, a mitochondrial Mn-superoxide dismutase. Wild-type mature embryo sacs show ROS exclusively in the central cell, which appears to be the main source of ROS before pollination. Accordingly, *MSD1* shows a complementary expression pattern. *MSD1* expression is elevated in the egg apparatus at maturity but is downregulated in the central cell. The *oiwa* mutants are characterized by high levels of ROS detectable in both the central cell and the micropylar cells. Remarkably, egg apparatus cells in *oiwa* show central cell features, indicating that high levels of ROS result in the expression of central cell characteristic genes. Notably, ROS are detected in synergid cells after pollination. This ROS burst depends on stigma pollination but precedes fertilization, suggesting that embryo sacs sense the imminent arrival of pollen tubes and respond by generating an oxidative environment. Altogether, we show that ROS play a crucial role during female gametogenesis and fertilization. MSD1 activity seems critical for maintaining ROS localization and important for embryo sac patterning.

INTRODUCTION

Reactive oxygen species (ROS) are emerging as signaling molecules that regulate many developmental and physiological responses in diverse organisms. In plants, ROS are implicated in a wide range of processes, including environmental responses, growth, cell elongation, apical dominance, tracheary element maturation, trichome development, senescence, programmed cell death, response to stress, and hormonal signaling (Joo et al., 2001; Rodríguez et al., 2002; Foreman et al., 2003; Carol and Dolan, 2006; Gapper and Dolan, 2006; Van Breusegem and Dat, 2006; Lee et al., 2007; Miller et al., 2008; De Tullio et al., 2010; Tsukagoshi et al., 2010; Kaye et al., 2011). Furthermore, growing evidence supports a crucial role for ROS in plant cell division: ROS were reported to accelerate auxin-mediated cell cycle entry in alfalfa (*Medicago sativa*) (Fehér et al., 2008) and to regulate the transition between cell proliferation and differentiation in *Arabidopsis thaliana* roots (Tsukagoshi et al., 2010).

[1] Address correspondence to gpagnussat@mdp.edu.ar.
The author responsible for distribution of materials integral to the findings presented in this article in accordance with the policy described in the Instructions for Authors (www.plantcell.org) is: Gabriela Carolina Pagnussat (gpagnussat@mdp.edu.ar).
[C] Some figures in this article are displayed in color online but in black and white in the print edition.
[W] Online version contains Web-only data.
www.plantcell.org/cgi/doi/10.1105/tpc.113.109306

On the other hand, ROS can also be cytotoxic, causing oxidative damage to cell structures and molecules and inducing cell death programs (Van Breusegem and Dat, 2006). This dual role of ROS acting as toxic agents or as signaling molecules is mainly dependent on concentration, pulse duration, and site of action. ROS fluctuations and homeostasis are thus tightly regulated in the plant cell. Such regulation is provided by a complex network of ROS production and scavenging that operates in all subcellular compartments (Mittler et al., 2004).

Superoxide dismutases (SODs; EC 1.15.1.1) catalyze the dismutation of superoxide to molecular oxygen and peroxide (H_2O_2) and are key components of the ROS gene network in plants, as they constitute the first line of cellular defense against ROS (Perl-Treves and Galun, 1991; Alscher et al., 2002). Most plants contain a number of SOD isozymes that are classified by their metal cofactors into three known types: iron SOD (FeSOD), manganese SOD (MnSOD), and copper-zinc SOD (Cu/ZnSOD). Three FeSOD genes (*FSD1*, *FSD2*, and *FSD3*), three Cu/ZnSOD genes (*CSD1*, *CSD2*, and *CSD3*) and one MnSOD gene (*MSD1*) are encoded in the *Arabidopsis* genome (Kliebenstein et al., 1998). Subcellular localization studies have suggested that FSD and CSD2 are localized in chloroplasts and that CSD1, CSD3, and MSD1 are localized in the cytoplasm, peroxisome, and mitochondria, respectively (Bowler et al., 1994).

Plant MnSODs are highly conserved; mature plant MnSOD proteins share ~65% identical sites and ~80% similarity. The less conserved ~25 first amino acids in the N-terminal region

correspond to the mitochondria localization signal peptide, which is processed and absent in the mature protein (Figure 1A).

The role of plant mitochondrial MSD1 has been mostly related to oxidative stress tolerance, as determined by studying transgenic plants overexpressing *MSD1* in various compartments (Van Breusegem et al., 1999; Samis et al., 2002; Wang et al., 2004; Y.C. Wang et al., 2010). However, although MSD1 was proposed to be a key component of the ROS regulatory network, its role in regulating ROS homeostasis during development is poorly understood. Only a few studies have examined its participation during plant growth or development. *Arabidopsis* antisense lines with decreased *MSD1* expression showed retarded root growth (Morgan et al., 2008), and a high-throughput forward genetic screen to find gametophytic mutants in *Arabidopsis* identified a transposon insertion line in *MSD1* (named MEE33 for MATERNAL EFFECT EMBRYO ARREST33) that was classified as a female gametophytic mutant, as it showed defects in female transmission (Pagnussat et al., 2005). Here, we show that ROS levels are tightly regulated during megagametogenesis. Oxidative bursts are only detected at specific stages of development and in very restricted locations. *MSD1* is expressed thorough the embryo sac, but it is downregulated in the central cell, which appears to be the main source of ROS in the mature female gametophyte before pollination. Functional characterization of two independent T-DNA insertional lines allelic to MEE33 revealed a role for MSD1 as an essential protein regulating ROS levels during female gametogenesis. As ROS homeostasis disruption in the mutant embryo sacs results in infertility or in arrested embryogenesis, we decided to name the mutant *oiwa*, after the main character of the Japanese ghost story Oiwa, who was poisoned by her husband and died, killing her unborn baby. In addition to an abnormal distribution of ROS along the embryo sacs, *oiwa* mutants show gametophytes in which egg apparatus cells seem to acquire central cell features, expressing central cell–specific markers and showing high levels of both mitochondrial superoxide and cytosolic ROS. Furthermore, a fraction of *oiwa* mutants showed mitotic arrest. Interestingly, ROS levels are also increased in synergid cells after pollination, suggesting that the embryo sacs perceive pollen tube approximation and prepare for its arrival by generating an oxidative burst. Thus, this report reveals a role for ROS as regulatory molecules affecting both gametophytic cell features and fertilization. *MSD1* expression in the embryo sac appears critical, as MSD1 restricts central cell fate and regulates ROS homeostasis, which is important for key aspects of embryo sac development, such as cell division progression, nuclei migration, and cell fate decisions.

RESULTS

Arabidopsis Lines with Insertions in *MSD1* Present Aberrant Female Gametophytes

To analyze *MSD1* function, two *Arabidopsis* lines (Columbia-0 [Col-0] ecotype) with T-DNA insertions located at exon 1 (*oiwa-1*) and in the promoter region (*oiwa-2*) were characterized (Figure 1 B). These lines were backcrossed to the Col-0 ecotype, and the genotype of the progeny from self-crossed plants was examined by PCR-based genotyping. No homozygous mutant plants were recovered in the offspring from either *oiwa-1/OIWA* or *oiwa-2/OIWA* self-pollinated plants. The ratio of heterozygous to wild-type plants was 0.51:1 for *oiwa-1/OIWA* (n = 338) and 0.48:1 for *oiwa-2/OIWA* plants (n = 454). As we could not recover any homozygous *oiwa* plants, only heterozygous *oiwa/OIWA* mutants were analyzed. No obvious growth or developmental defects were observed in the

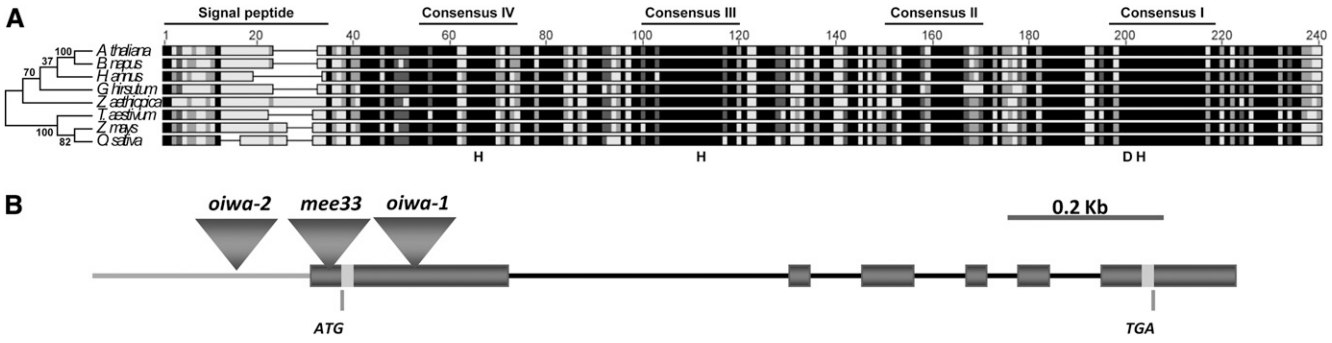

Figure 1. *OIWA* Encodes a Highly Conserved Mn-SOD.

(A) Eight representative sequences, four dicots (*Arabidopsis thaliana*, *Brassica napus*, sunflower [*Helianthus annuus*], and cotton [*Gossypium hirsutum*]) and four monocots (*Zantedeschia aethiopica*, wheat [*Triticum aestivum*], maize [*Zea mays*], and rice [*Oryza sativa*]) are schematized. Four conserved amino acid residues, which are critical for Mn-SOD function, are indicated (His-64, His-112, His-205, and Asp-201 in the consensus sequence). Residue conservation is represented along the sequences using a color code (black, 100% identical; dark gray, 80 to 100% similarity; gray, 60 to 80% similarity; white, <60% similarity). Consensus I-IV and signal peptide regions are indicated. The unrooted phylogenetic tree shown was constructed using the neighbor-joining method. The percentage of replicate trees in which the associated taxa clustered together in the bootstrap test (1000 replicates) is shown next to the branches. The evolutionary distances were computed using the Poisson correction method and are in the units of the number of amino acid substitutions per site. Evolutionary analyses were conducted in MEGA5.

(B) Structure of At3g10920 gene (*OIWA*). Exons (dark gray boxes), introns (black lines), promoter region (gray line), ATG and TGA (gray box), and the localization of the *oiwa-1*, *oiwa-2*, and *mee33* insertions are indicated.

heterozygous plants, suggesting that *oiwa* is a recessive mutation in the sporophyte. However, siliques of *oiwa/OIWA* plants showed a reduced seed set of ~50% (51.23% for *oiwa-1/OIWA* and 49.71% for *oiwa-2/OIWA*; Figure 2), suggesting that the gene is essential for gametogenesis and/or seed development.

To determine the genetic basis for this phenomenon, we crossed heterozygous plants as either pollen or egg donors to wild-type plants from the Columbia accession, and the transmission efficiency (TE = mutant/wild-type offspring) of *oiwa* was determined (Table 1). TE represents the fraction (%) of mutant alleles that are successfully transmitted. Only ~15% of megagametophytes carrying *oiwa-1* and ~8% megagametophytes carrying *oiwa-2* successfully transmitted the mutation, demonstrating that *oiwa* affects female gametophyte development or function. TE through the pollen was ~72% for *oiwa-1* and 80% for *oiwa-2*, indicating that male gametophytes are only slightly affected by the mutation (Table 1).

To analyze the basis of the female transmission deficiency, the terminal phenotype of gametophytes from emasculated *oiwa/OIWA* flowers was studied. By emasculating the flowers, we allowed wild-type embryo sacs to reach the final stage of development (FG7; Figure 3A) (Christensen et al., 1998). In wild-type *Arabidopsis*, the female gametophyte or embryo sac is a seven-cell structure that includes two gametic cells, the egg cell and the central cell, and five accessory cells. The egg cell is located at the micropylar end of the embryo sac and is flanked by two synergid cells, responsible for pollen tube attraction, forming the egg apparatus (Pagnussat et al., 2005; Okuda et al., 2009). The second gametic cell, the central cell, occupies most of the female gametophyte and initially includes two haploid polar nuclei that fuse before fertilization, generating a diploid nucleus. Three antipodal cells are located at the chalazal end of the embryo sac. Their function is still unclear, and they undergo programmed cell death before fertilization. The whole gametophytic structure originates from a haploid megaspore that differentiates inside the ovule primordium. Three successive nuclear division cycles originate a syncytium of eight nuclei. Further differentiation gives rise to the seven cells that comprise the embryo sac (see Supplemental Figure 1 online). *oiwa* gametophytes showed variable defects, ranging from embryo sacs arrested at early stages of development (two nuclei stage or FG2-FG3; Christensen et al., 1997) to gametophytes with aberrant egg apparatus, probably due to a variable penetrance of the mutation in the female gametophyte (see Supplemental Table 1 online). In *oiwa-1/OIWA* pistils, 54.6% of the ovules carried normal mature embryo sacs (Figure 3B). Twenty-one percent of the embryo sacs displayed mitotic arrest: The majority of them (14.3% of all the embryo sacs analyzed) were arrested at the four nuclei stage (FG4; Figure 3D), while the rest were arrested at the two nuclei stage (FG3; Figure 3C). Interestingly, 4.6% of all the embryo sacs showed aberrant egg apparatuses. While in wild-type embryo sacs, the two synergid nuclei are observed at the micropylar pole of the embryo sac and the egg cell nucleus is positioned at the chalazal pole of the cell, some *oiwa* embryo sacs showed two cells with egg cell cytological features instead of one, and only one nucleus was detected at the typical synergid position (Figure 3E). The last phenotypic class observed includes embryo sacs in which the polar nuclei failed to fuse (19.6% of the embryo sacs; Figure 3F). Similar phenotypes and distribution were observed when *oiwa-2/OIWA* pistils were analyzed (see Supplemental Figure 2 online). Additionally, we also studied the phenotype of ovules in *oiwa-1/OIWA* pistils 2 d after pollination with wild-type pollen. Out of 280 ovules analyzed, 151 (53.9%; Figure 4A; see Supplemental Table 2 online) showed an embryo at the one-cell stage, 76 (27.1%; Figure 4B; see Supplemental Table 2 online)

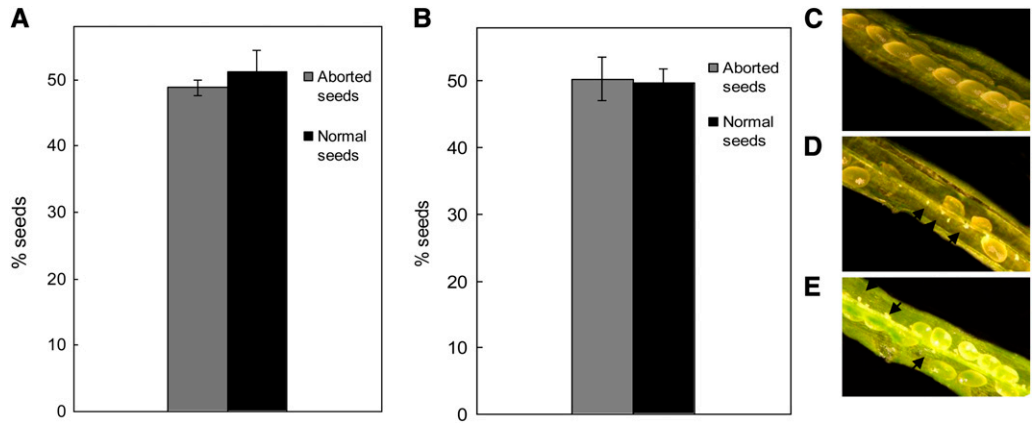

Figure 2. *oiwa* Mutants Have Reduced Seed Sets.

(A) Percentage of aborted seeds in siliques from *oiwa-1/OIWA* plants (n = 316)
(B) Percentage of aborted seeds in siliques from oiwa-2/OIWA plants (n = 515).
(C) Dissected wild-type silique of a wild-type plant showing viable seeds.
(D) *oiwa-1/OIWA* silique at a comparable stage. Aborted ovules are indicated by arrows.
(E) *oiwa-2/OIWA* silique at a comparable stage. Aborted ovules are indicated by arrows.
Error bars indicate SE. The percentage of aborted seeds in siliques from wild-type plants was 3.13% (n = 543).
[See online article for color version of this figure.]

Table 1. TE of *oiwa* Mutants

Parental Genotypes (Female × Male)[a]	Antibiotic Resistant (Ant^r)	Antibiotic Sensitive (Ant^s)	TE[b]
OIWA/OIWA × *oiwa-1/OIWA*	39	54	72.22%
oiwa-1/OIWA × *OIWA/OIWA*	17	116	14.65%
OIWA/OIWA × *oiwa-2/OIWA*	67	83	80.72%
oiwa-2/OIWA × *OIWA/OIWA*	8	98	8.16%

[a]Plants were crossed manually, and seeds of the resulting cross were collected and grown on selective Murashige and Skoog plates to determine the efficiency in which the mutant allele was transmitted to the next generation by the male or female gametes. Selective plates to assay transmission of *oiwa-1* contained 50 mg·L^{-1} kanamycin, while selective plates to assay transmission of *oiwa-2* contained 15 mg·L^{-1} sulfadiazine.
[b]TE = Ant^r/Ant^s × 100%.

showed embryogenesis arrested at the zygotic stage, with endosperm development affected as well, and 53 ovules showed collapsed embryo sacs, probably arising from those that were previously found to display mitotic arrest. These findings also suggest that a proportion of the mutant embryo sacs that showed later gametophytic defects 2 d after emasculation were capable of completing their developmental program and were able to get fertilized, although fertilization resulted in early seed abortion due to a gametophytic maternal effect. To study the fertilization success of *oiwa* embryo sacs, we pollinated wild-type and *oiwa-1/OIWA* pistils using pollen from plants carrying the *PFAC1IE*:*GFP-GUS*:*TFAC1* construct, and β-glucuronidase (GUS) expression was examined in the ovules after pollination. *EMBRYONIC FACTOR1* (*FAC1*) encodes an AMP deaminase (EC:3.5.4.6) and is expressed from the paternal allele in both the developing embryo and endosperm (Xu et al., 2005). While in wild-type pistils 92% of the ovules showed GUS expression (n = 233), the percentage of fertile ovules in *oiwa-1/OIWA* pistils was 69% (n = 198; Figure 4C). This result suggests that ~38% of the mutant embryo sacs are able to get fertilized.

oiwa Female Gametophytes Have Abnormal Cellular Differentiation

To further characterize the differentiation status and identities of the cells in *oiwa* embryo sacs, we analyzed the expression of cell-specific molecular markers. The marker lines were crossed with both wild-type plants and *oiwa-1* mutant plants, and the F1 progeny were analyzed for expression of the marker genes. When the expression of the egg cell–specific marker ET1119 (Gross-Hardt et al., 2007) was analyzed in wild-type pistils hemizygous for the marker, its expression was detected in

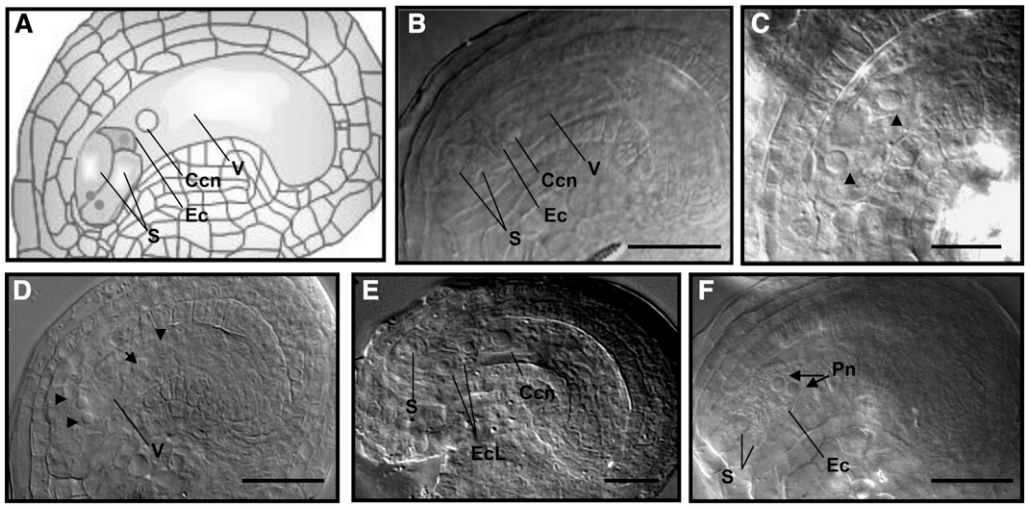

Figure 3. Female Gametogenesis Is Impaired in *oiwa-1* Mutants.

(A) Scheme showing a mature wild-type embryo sac at FG7.
(B) Image of a properly developed embryo sac from an *oiwa-1/OIWA* pistil at FG7.
(C) Embryo sac arrested at FG3 stage showing two nuclei (arrowheads) separated by a vacuole.
(D) Embryo sac arrested at the FG4 stage. One pair of nuclei is located at each side of the vacuole (arrowheads).
(E) Embryo sac showing an abnormal egg apparatus.
(F) Embryo sac showing unfused polar nuclei (arrows).
Ccn, central cell nucleus; Ec, egg cell; Pn, polar nuclei; S, synergid cells; V, vacuole. A total of 280 ovules were analyzed. Bars = 10 μm in **(C)** and **(D)** and 25 μm in **(B)**, **(E)**, and **(F)**.

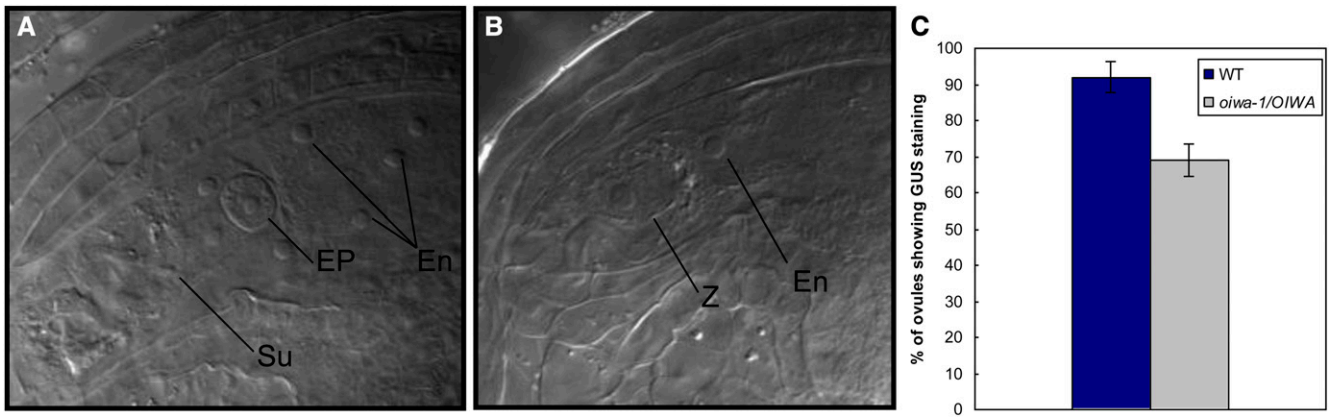

Figure 4. Postpollination Phenotype of *oiwa* Embryo Sacs.

(A) Wild-type ovule showing a developing embryo at one-cell stage and developing endosperm.
(B) Embryo sac from an *oiwa-1/OIWA* pistil showing embryogenesis arrested at the zygotic stage.
(C) Fertilization success of *oiwa* embryo sacs is impaired as evidenced by the percentage of ovules showing expression of the paternal marker *PFAC1IE*:*GFP-GUS*:*TFAC1* after pollination (n = 233 for wild-type [WT] pistils and 198 for *oiwa-1/OIWA* pistils). En, endosperm nucleus; EP, embryo proper; Su, suspensor; Z, zygote. Error bars indicate SE.
[See online article for color version of this figure.]

41.4% of the ovules and exclusively in the egg cell (n = 186; Figure 5A). However, when its expression was tested in *oiwa-1/OIWA* pistils, only 28.9% of the embryo sacs showed a normal expression pattern in the egg cell, while 8.4% of all embryo sacs presented strong expression in two to three cells of the egg apparatus (egg cell–like cells, n = 214; Figure 5B), suggesting that at least two egg cells are specified in a fraction of the *oiwa* embryo sacs.

When expression of the synergid cell–specific marker ET884 (Gross-Hardt et al., 2007) was analyzed in wild-type pistils, two micropylar cells were GUS positive in 43.4% of the embryo sacs (n = 129; Figure 5C). In *oiwa-1/OIWA* pistils, 31.7% of ovules were positive for GUS staining. However, 6.3% of the ovules showed GUS expression in just one micropylar cell (n = 221; Figure 5D).

Central cell–specific marker DD65 expression was also studied (Steffen et al., 2007; Leshem et al., 2012). Forty-three percent of the embryo sacs showed green fluorescent protein (GFP) expression specifically in the central cell in wild-type pistils hemizygous for the marker (n = 178; Figure 5E). When expression of the marker was tested in *oiwa-1/OIWA* pistils, 38.2% of the ovules were positive for GFP (n = 226). Around 24% (23.7%) of the ovules showed GFP expression restricted to the central cell of the embryo sac, while the remaining 14.5% of the female gametophytes displayed GFP expression not only in the central cell but widespread throughout the micropylar cells of the embryo sacs (Figure 5F). Additionally, expression of the nuclear-localized central cell–specific marker *pMEA*:*NLS*:*GUS* (Kägi et al., 2010) was studied in both wild-type and *oiwa-1/OIWA* pistils. *pMEA*:*NLS*:*GUS* was expressed in 44.3% of the ovules in wild-type pistils hemizygous for the marker (n = 199; Figure 5G). When expression of *pMEA*:*NLS*:*GUS* was studied in *oiwa-1/OIWA* pistils, 37.3% of the ovules were positive for GUS (n = 204). Around 26% (25.8%) of the ovules showed GUS expression restricted to the central cell nucleus of the embryo sac, while the remaining 11.5% of the female gametophytes displayed GUS expression not only in the central cell nucleus but also in all three micropylar nuclei (Figure 5H).

When expression of the antipodal-specific cell marker *pAt1g36340*:*GUS* was studied in wild-type pistils, 32.3% of the embryo sacs showed GUS expression at the antipodal region (n = 235). In the case of *oiwa-1/OIWA* pistils, 29.4% of the embryo sacs exhibited GUS expression in antipodal cells and no abnormal patterns of expression were detected, suggesting that antipodal specification was not affected in the *oiwa* embryo sacs that reached maturity (n = 204; see Supplemental Figure 3 online).

Together, these results suggest that OIWA is important for normal patterning of the embryo sac and for restricting central cell identity.

ROS Surround the Central Cell Nucleus in Wild-Type Female Gametophytes before Fertilization, and Their Level and Distribution Are Altered in *oiwa* Embryo Sacs

The fact that mutations in *OIWA* lead to gametophytic effects that include mitotic arrest and cell misspecification suggests that mitochondrial superoxide levels need to be tightly regulated during the female gametophyte developmental program. MSD1's dismutase activity might be required to regulate ROS homeostasis along the different stages of megagametogenesis. To test this hypothesis, we studied ROS levels during female gametogenesis in both wild-type and *oiwa* embryo sacs by confocal microscopy using emasculated flowers. To analyze overall intracellular ROS levels, we used the fluorescent probe 5-(and 6)-carboxy-2′,7′-dichlorodihydrofluorescein diacetate (Molecular Probes). 5-(and 6)-Carboxy-2′,7′-dichlorodihydrofluorescein diacetate diffuses rapidly into the cells where it is hydrolyzed to 2′,7′-dichlorofluorescin (DCFH). Although it is generally accepted that DCFH is trapped in the cytosol where it

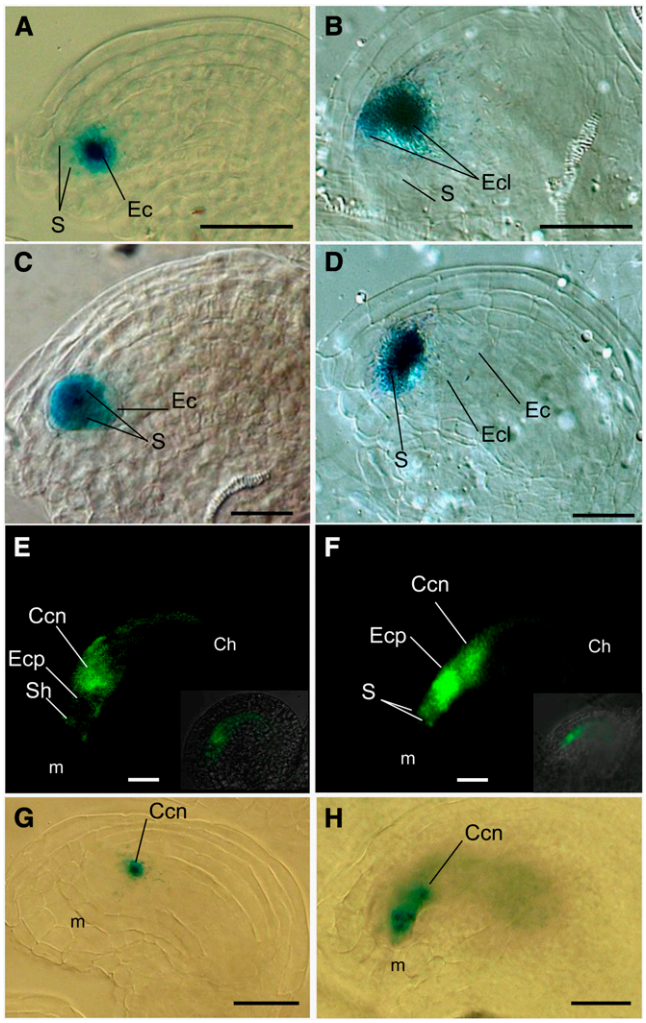

Figure 5. Aberrant Differentiation of Cell Types in *oiwa-1* Embryo Sacs.

(A) Expression of the specific egg cell marker ET1119 in a wild-type embryo sac.

(B) The egg cell marker ET1119 is expressed in two micropylar cells in an *oiwa* embryo sac.

(C) Expression of the specific synergid cell marker ET884 in a wild-type embryo sac.

(D) The synergid cell marker ET884 is expressed in only one micropylar cell in an *oiwa* embryo sac.

(E) Expression of the specific central cell marker DD65 in a wild-type embryo sac. Inset shows the fluorescence micrograph merged with its DIC image.

(F) The central cell specific marker DD65 is widely expressed in *oiwa* embryo sacs. Signal is detected at both the micropylar cells and at the chalazal region of the female gametophyte. Inset shows the fluorescence micrograph merged with its DIC image.

(G) Expression of the specific central cell marker *pMEA*:*NLS*:*GUS* in a wild-type embryo sac.

(H) The central cell specific marker *pMEA*:*NLS*:*GUS* is ectopically expressed in egg cell and synergid cells nuclei in embryo sacs from *oiwa-1/OIWA* pistils.

Ccn, central cell nucleus; Ch, chalaza; Ec, egg cell; Ecl, egg cell like; Ecp, egg cell position; m, micropyle; S, synergid; Sh, synergid hook. Bars = 25 μm.

is oxidized by a variety of ROS, preferentially hydrogen peroxide, to the highly fluorescent 2′,7′-dichlorofluorescein (DCF), colocalization of DCF fluorescence with mitochondria has also been reported (Zhang et al., 2009; Bi et al., 2012). As DCFH is rather insensitive to superoxide, DCF signal is generally correlated with peroxide levels (Royall and Ischiropoulos, 1993; Myhre et al., 2003). Mitochondrial superoxide levels were studied using MitoSOX red, a mitochondrial superoxide indicator (Invitrogen) that is selectively targeted to mitochondria and is fluorescent upon oxidation (Robinson et al., 2006). When both probes were used simultaneously on wild-type pistils, a strong signal was detected at FG0, during megaspore cell death (see Supplemental Figure 4 online). The signal detected corresponded only to DCF fluorescence, while we were not able to detect a MitoSOX signal, which indicates that mitochondrial superoxide is not produced during megaspore cell death. As the DCF signal detected might correspond to other mitochondrial ROS besides superoxide, we used MitoTracker red in addition to H_2DCFDA to see if the DCF signal detected colocalized with mitochondria. As can be observed in Supplemental Figure 4 online, the DCF signal did not colocalize with MitoTracker red fluorescence, suggesting that ROS are accumulated in other subcellular compartments. A strong signal was also detected later in development around the central cell nucleus in embryo sacs at stage FG6-FG7, a step in which antipodal cells undergo programmed cell death. However, no signal was detected in the antipodal region. An overlap between H_2DCFDA and MitoSOX red staining was observed, indicating that not only superoxide but also other ROS (detected by H_2DCFDA) are present in mitochondria (Figures 6A to 6D). This was confirmed by double staining experiments using both H_2DCFDA and MitoTracker red, which showed colocalization of DCF and MitoTracker fluorescence (see Supplemental Figure 4 online). ROS could also be detected outside the mitochondria (green fluorescence detected in overlay images; Figure 6C; see Supplemental Figure 4 online). Neither H_2DCFDA nor MitoSOX signals were detected when other stages of wild-type gametophyte development were analyzed (see Supplemental Figure 4 online). When ovules from *oiwa-1/OIWA* pistils were studied for ROS levels during early stages of development, no differences in comparison with wild-type embryo sacs were detected. However, from stage FG5 on, ROS could be detected inside the female gametophyte (see Supplemental Figure 4 online). At stage FG6-FG7, ROS were detected not only in the whole central cell but also at the micropylar region of the embryo sac in 71 out of 191 ovules analyzed (37.1%), and a significant overlap between H_2DCFDA and MitoSOX red signal was also observed (Figures 6E to 6H; see Supplemental Figure 4 online). From the ovules showing extended ROS signals along the embryo sacs, 36.6% corresponded to collapsing ovules (see Supplemental Figure 4 online), while the remaining 63.34% corresponded to ovules with embryo sacs that were undistinguishable in shape and size from the ones exhibiting wild-type-like ROS distribution. These experiments indicate that in the absence of MSD1, ROS accumulation is no longer restricted to the domain around the central cell nucleus, as they are detected in the egg apparatus as well. Also, not only did superoxide accumulate in the mutant gametophytic mitochondria, but other ROS also increased inside the

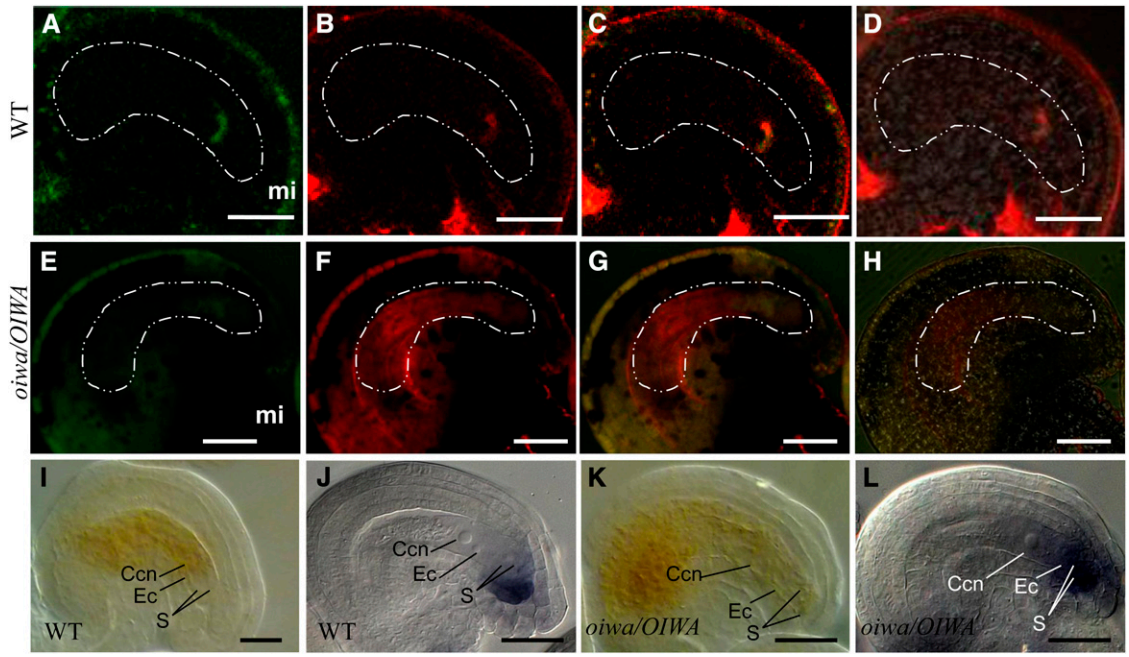

Figure 6. ROS in *Arabidopsis* Embryo Sacs from Wild-Type or *oiwa-1/OIWA* Pistils from Emasculated Flowers.

(A) to **(D)** Ovule from a wild-type (WT) pistil showing H_2DCFDA **(A)** or MitoSOX **(B)** fluorescence inside the embryo sac, around the central cell; **(C)** shows the overlaid fluorescence of H_2DCFDA and MitoSOX. **(D)** Shows the overlaid of fluorescence with the DIC image.

(E) to **(H)** Ovule from an *oiwa-1/OIWA* pistil showing H_2DCFDA **(E)** or MitoSOX **(F)** fluorescence inside the embryo sac. Note fluorescence all along the female gametophyte. **(G)** shows the overlaid fluorescence of H_2DCFDA and MitoSOX. **(H)** shows the overlaid of fluorescence with the DIC image.

(I) Ovule from a wild-type pistil showing DAB staining in the central cell of the embryo sac.

(J) NBT staining in an ovule from a wild-type pistil. Cytosolic superoxide is detected outside the embryo sac in the micropylar portion of the ovule integuments.

(K) Ovule from an *oiwa-1/OIWA* pistil showing DAB staining all along the embryo sac.

(L) NBT staining in an ovule from an *oiwa-1/OIWA* pistil. Cytosolic superoxide is detected inside the embryo sac, principally at the micropylar region of the gametophyte.

The embryo sacs are delimited by a dashed line. Ccn, central cell nucleus; Ec, egg cell; mi, indicates micropyle, S, synergid cells. Bars = 25 μm.

organelle (as MitoSOX red and DCF signals colocalized) and in what appears to be the nearby cytosolic space.

To further investigate the nature of the ROS present in the embryo sacs, we incubated both wild-type and *oiwa-1/OIWA* pistils in nitroblue tetrazolium (NBT) to look for cytosolic superoxide, and we also incubated the pistils in diaminobenzidine tetrahydrochloride (DAB) to detect H_2O_2. Cytosolic superoxide was only detected outside the embryo sac in ovules from unpollinated wild-type pistils, specifically at the micropylar end of the inner integument adaxial side (Figure 6J). In the case of DAB, staining could only be observed in the central cell of unfertilized wild-type embryo sacs and was excluded from the sporophytic tissues of the ovule. When ovules from *oiwa-1/OIWA* pistils were examined for DAB staining, 66 out of 186 ovules (35.4%) showed DAB staining spread all over the embryo sac, while the remaining 120 ovules showed a pattern similar to the one observed for wild-type ovules (Figures 6I and 6K). Again, no staining was observed in the sporophytic tissues surrounding the embryo sac. NBT staining for superoxide in *oiwa-1/OIWA* pistils showed that 79 ovules out of 215 (36.7%) presented cytosolic superoxide localized not only in the inner integument but also inside the embryo sac, more specifically in synergid cells and in the egg cell. The remaining ovules (63.2%) exhibited NBT staining confined to the inner integument of the ovule resembling the pattern observed for wild-type ones (Figures 6J and 6L).

Thus, specific ROS seem to prevail at each of the different tissues comprising the ovule. The unusual staining patterns observed in ovules from *oiwa-1/OIWA* pistils suggest that MSD1 is required not only to regulate mitochondrial ROS levels inside the female gametophyte, but also to regulate cytoplasmic ROS homeostasis along the whole embryo sac.

An Oxidative Burst in Synergid Cells Precedes Pollen Tube Arrival in Wild-Type Embryo Sacs

ROS distribution during embryo sac fertilization was investigated in embryo sacs from wild-type and *oiwa-1/OIWA* pistils after controlled manual pollination with wild-type pollen using the same probes and staining described above. When wild-type pistils were dissected 5 h after pollination (HAP), a time point in which the majority of the gametophytes are not yet fertilized (see Supplemental Figure 5 online; Sandaklie-Nikolova et al., 2007), MitoSOX red signal was not longer detected in the central

cell of the embryo sacs. However, a strong signal corresponding to DCF fluorescence was observed at the micropylar edge of the synergid cells, more precisely at a structure formed by cell wall projections into the synergid cytoplasm called the filiform apparatus (FA; Figure 7A). Twelve hours after fertilization, a pollen tube that reached the micropyle of the embryo sacs was present in nearly all ovules in the pistils (~94%, *n* = 187; see Supplemental Figure 5 online). At this point, both DCF fluorescence and MitoSOX red signals were detected at one of the synergid cells (Figure 7B). Twenty-four hours after pollination, 98% of the ovules in wild-type pistils showed fertilized embryo sacs (*n* = 221), and neither DCF nor MitoSOX red signal was detected inside the embryo sacs (Figure 7C). When cytosolic superoxide was studied 5 HAP, no NBT staining was detected inside the embryo sacs (Figure 7G). However, intense staining was detected in the synergid cells 12 HAP, overlapping the region where a strong DCF fluorescence signal was previously detected (Figures 7B and 7H). After fertilization, cytosolic superoxide is excluded again from the embryo sac, as NBT staining could only be observed in the micropylar end of the integuments (Figure 7I). At 5 HAP, DAB staining was detected in the central cell, with less intensity in the synergid cells. Strong staining was also detected in the chalazal area of the ovule just outside the embryo sac (Figure 7M). When the pollen tube arrived at the ovule 12 HAP, DAB staining indicated that peroxide was present principally in the antipodal cell region, probably as a consequence of antipodal cell death (Figure 7N). DAB staining in the central cell and in the synergid cells was less evident. After fertilization, DAB staining was excluded from the embryo sac. All together, these results suggest that both cytosolic and mitochondrial superoxides are the prevalent ROS that accumulate in the synergid cells upon pollination.

When *oiwa-1/OIWA* pistils were dissected 5 HAP, 14.2% of the ovules were found to have collapsed, and 60.3% of the ovules had embryo sacs exhibiting only DCF signals in the FA, as observed in embryo sacs from wild-type pistils, while 25.5% of the ovules showed both DCF signals and mitochondrial superoxide along the embryo sac, but predominantly in the FA (*n* = 157; Figure 7D). In these ovules, DCF signals and mitochondrial superoxide were also detected in the sporophytic tissue surrounding the embryo sac. Twelve hours after pollination of *oiwa-1/OIWA* pistils, 15.1% of the ovules were found to have collapsed, while 55.4% showed ROS in one of the synergid cells, as observed for wild-type ovules, and 29.5% of the ovules had embryo sacs that were undistinguishable from those of wild-type ovules in shape and size but exhibited both DCF (green) and MitoSOX (red) signals. These signals were detectable inside the embryo sac but were strong in one of the synergid cells (*n* = 258; Figure 7E). Even when these ovules showed not only DCF signals, but also mitochondrial superoxide in the synergid cells, they seemed to be able to attract pollen tubes (Figure 7E). When *oiwa-1/OIWA* pistils were dissected 24 HAP, 57% of the ovules showed no detectable fluorescence inside the embryo sacs, as observed in wild-type ovules. However, 15.5% were found to be collapsed, and the remaining 27.5% exhibited high levels of both cytosolic ROS and mitochondrial superoxide not only all along the embryo sac but also in the sporophytic tissues of the ovule (*n* = 149; Figure 7F). Those ovules were similar in size and shape to the ones that appeared to be fertilized but lacked fluorescence.

When cytosolic superoxide was studied 5 HAP in *oiwa-1/OIWA* pistils, 28 ovules out of 168 (16.6%) were collapsed and exhibited NBT staining throughout the embryo sac and sporophytic tissue. Eighty-nine ovules (53%) presented a NBT staining pattern that was similar to the one observed for wild-type ovules, while the remaining ovules (36%) presented NBT staining inside the embryo sac, particularly at the egg apparatus and at the adaxial side of the inner integument (Figure 7J). Twelve hours after pollination of *oiwa-1/OIWA* pistils, 32 ovules out of 179 (17.9%) were found to be collapsed. In addition, 93 ovules (52%) showed cytosolic superoxide at the two synergid cells as observed for wild-type ovules (Figure 7H), while 54 ovules (30.1%) showed a wider distribution of cytosolic superoxide with strong staining in the egg apparatus of the embryo sacs (Figure 7K). When *oiwa-1/OIWA* pistils were analyzed 24 HAP, 20.5% of the ovules were found to be collapsed, while 113 of the ovules (61.1%) showed a staining pattern that was undistinguishable from the one observed in wild-type embryo sacs, and the remaining 18.3% presented high levels of cytosolic superoxide all along the fertilized embryo sac and the sporophytic tissues of the ovule (*n* = 185; Figure 7L). When *oiwa-1/OIWA* pistils were studied for peroxide content 5 HAP, 27.1% of the ovules showed DAB staining all over the embryo sac, with more intensity in the chalazal zone of the embryo sac (Figure 7P). A fraction of the embryo sacs was found to be collapsed at this stage (17.5%), while the rest of the ovules (55.4%) showed a staining pattern similar to the one observed for wild-type ovules (*n* = 114; Figure 7M). Twelve hours after pollination of *oiwa-1/OIWA* pistils, 21.5% of the ovules were found to be collapsed, while the rest of the ovules analyzed (78.4%) exhibited hydrogen peroxide spread all over the embryo sac with more intensity in the antipodal zone and could not be differentiated from the pattern of DAB staining exhibited by wild-type ovules (*n* = 188; Figure 7N and 7Q). When *oiwa-1/OIWA* pistils were dissected 24 HAP, peroxide was excluded from the embryo sac in 60.2% of the ovules. A total of 18 ovules (19.3%) were found collapsed, while the remaining ovules (20.4%) presented high levels of peroxide all over the fertilized embryo sac and the surrounding sporophytic tissue (*n* = 193; Figure 7R).

The Aberrant Cell Specification in *oiwa* Embryo Sacs Is Not Related to a Disturbed Auxin Gradient inside the Female Gametophytes

Determination of cell fate inside the embryo sac relies on a location-specific mechanism (Evans, 2007; Pagnussat et al., 2007). The phytohormone auxin was shown to provide positional information and thus to regulate cell specification in the female gametophyte of *Arabidopsis* (Pagnussat et al., 2009). The distribution of auxin response, which was examined by observing the expression of the synthetic auxin-responsive reporter *DR5*:*GFP* (Ulmasov et al., 1997), showed a highly asymmetric distribution inside the developing embryo sac, exhibiting a maximum at the micropylar end (Pagnussat et al., 2009). ROS are known to affect auxin homeostasis at different

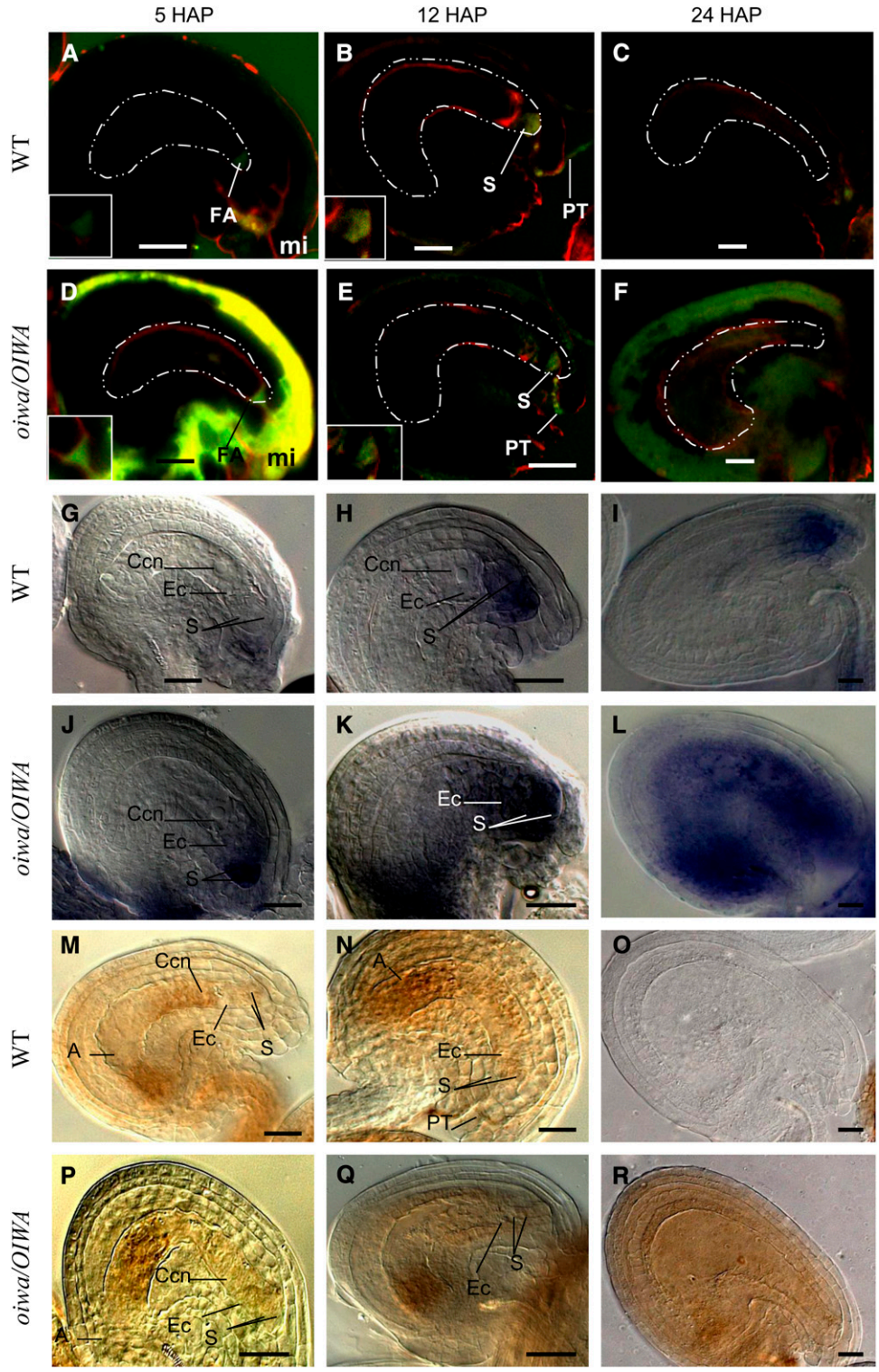

Figure 7. ROS in *Arabidopsis* Embryo Sacs from Wild-Type or *oiwa-1/OIWA* Pistils after Pollination with Wild-Type Pollen.

(A) Ovule from a wild-type (WT) pistil 5 HAP showing overlaid fluorescence of H_2DCFDA and MitoSOX. Both H_2DCFDA and MitoSOX fluorescence was observed at the FA. Inset shows an enlarged view of the micropyle.

(B) Overlaid fluorescence of H_2DCFDA and MitoSOX in an ovule from a wild-type pistil 12 HAP showing H_2DCFDA fluorescence in one of the synergid cells. ROS are also detected in the pollen tube that reached the ovule micropyle. Inset shows an enlarged view of the micropyle.

levels, by inducing its oxidative degradation or by affecting its polar transport (Gazarian et al., 1998; Jansen et al., 2001; Grunewald and Friml, 2010). As the auxin gradient may be disturbed during development in *oiwa* mutants due to the observed overflow of ROS, we studied the expression of the *DR5*:*GFP* auxin responsive reporter in embryo sacs at stage FG4-FG5 both in wild-type and in the *oiwa-1/OIWA* background. Embryo sacs in *oiwa-1/OIWA* pistils showed an asymmetrical *DR5*:*GFP* distribution, which was comparable to the one observed in gametophytes from wild-type pistils, indicating that the *oiwa* mutation did not affect the auxin response gradient (see Supplemental Figure 6 online). A total of 42.8 of auxin-gradient positive embryo sacs were observed in *oiwa-1/OIWA* pistils, while 48.2 were observed in pistils from wild-type plants (see Supplemental Figure 6 online). The difference observed between wild-type and *oiwa-1/OIWA* pistils can be explained by the fact that when wild-type embryo sacs are at the FG4-FG5 stage, a fraction of the *oiwa* embryo sacs are already arrested. In conclusion, an auxin gradient distortion does not seem to be responsible for the cell misspecification detected in *oiwa* embryo sacs.

Nuclei Migration Is Affected in *oiwa* Female Gametophytes

As explained above, cell specification along *Arabidopsis* embryo sacs was shown to depend on a positional mechanism (Pagnussat et al., 2007). As the auxin gradient was not affected by the *oiwa* mutation, we therefore analyzed how nuclei migration progresses in *oiwa* gametophytes. Nuclei migration defects were already shown to be related to misspecification of synergids to egg cells in the female gametophytic mutant *eostre* (Pagnussat et al., 2007). Wild-type and *oiwa* embryo sacs were analyzed at the FG5 stage, the eight nucleated stage at which the precise positioning of nuclei determines cell specification (Pagnussat et al., 2007; Srilunchang et al., 2010). We found that 5.6% of the ovules from *oiwa-1/OIWA* pistils showed abnormal distribution of nuclei along the embryo sac, with aberrant positioning of nuclei at the micropylar end of the gametophyte (n = 178; Figure 8). While wild-type embryo sacs showed two nuclei at the edge of the micropylar pole and one nucleus toward the middle area of the micropylar region, a percentage of *oiwa* mutant embryo sacs showed only one nucleus at the edge of the gametophyte and two nuclei instead of one at the region in which the egg cell nucleus should be specified (Figures 8A and 8B). This atypical arrangement of nuclei was never detected when wild-type pistils were analyzed (n = 237). No other abnormalities were observed in the rest of the nuclei comprising the embryo sac. This result suggests that the misspecification of the egg apparatus observed for a fraction of *oiwa* embryo sacs (4.8 to 8.4%; Figures 3 and 5) might arise from an atypical arrangement of nuclei at the micropylar region of the gametophyte as a result of nuclei migration defects.

Mitochondria Functionality Is Compromised in *oiwa* Female Gametophytes

The late defects in development observed in mutant embryo sacs, such as unfused polar nuclei or early embryogenesis arrest, might be due to the fact that high levels of superoxide could be affecting mitochondrial functionality in *oiwa* gametophytes. Supporting this idea, the mutant *fiona*, which shows central cells with altered mitochondria ultrastructure, was

Figure 7. (continued).

(C) ROS at 24 HAP are not longer detectable in fertilized wild-type embryo sacs.
(D) Overlaid fluorescence of H_2DCFDA and MitoSOX in an ovule from an *oiwa-1/OIWA* pistil 5 HAP. Both H_2DCFDA and mitochondrial superoxide signals (yellow fluorescence) are detected inside the embryo sac principally at the FA and in the sporophytic tissues of the ovule. Inset shows an enlarged view of the micropyle.
(E) Pollen tubes at 12 HAP reach the micropyle of mature ovules with abnormal ROS accumulation in *oiwa-1/OIWA* pistils. Both DCF and mitochondrial superoxide are detected inside the embryo sac. Inset shows an enlarged view of the micropyle.
(F) Ovule from an *oiwa-1/OIWA* pistil 24 HAP showing overlaid fluorescence of H_2DCFDA and MitoSOX. Both cytosolic ROS and mitochondrial superoxide are detected all along the fertilized embryo sac.
(G) Ovule from a wild-type pistil 5 h after pollination showing cytosolic superoxide stained with NBT outside the embryo sac.
(H) NBT staining in an ovule from a wild-type pistil 12 HAP showing superoxide in the synergid cells.
(I) Superoxide at 24 HAP seems excluded again from the fertilized embryo sac.
(J) NBT staining in an ovule from an *oiwa-1/OIWA* pistil 5 HAP. Cytosolic superoxide is detected inside the embryo sac principally at micropylar end.
(K) Ovule from an *oiwa-1/OIWA* pistil at 12 HAP showing NBT staining detectable in the egg cell and synergid cells.
(L) Ovule from an *oiwa-1/OIWA* pistil at 24 HAP showing cytosolic superoxide detectable all along the fertilized embryo sac.
(M) DAB staining in an ovule from a wild-type pistil at 5 HAP showing the presence of peroxide in the central cell. A weaker staining is also detected in the synergid cells.
(N) DAB staining in an ovule from a wild-type pistil at 12 HAP showing the presence of peroxide in the central cell, synergid cells, and antipodal region of the embryo sac.
(O) Peroxide at 24 HAP seems excluded from the female gametophyte.
(P) Ovule from an *oiwa-1/OIWA* pistil at 5 HAP showing DAB staining all over the embryo sac with more intensity in the chalazal zone.
(Q) Ovule from an *oiwa-1/OIWA* pistil at 12 HAP stained with DAB showing hydrogen peroxide spread all over the embryo sac with more intensity in the antipodal zone.
(R) Fertilized embryo sac from an *oiwa-1/OIWA* pistil showing DAB staining all over the female gametophyte and the sporophytic surrounding tissue. The embryo sacs are delimited by a dashed line. A, antipodal cells; Ccn, central cell nucleus; Ec, egg cell; mi, indicates micropyle; PT, pollen tube; S, synergid. Bars = 25 μm.

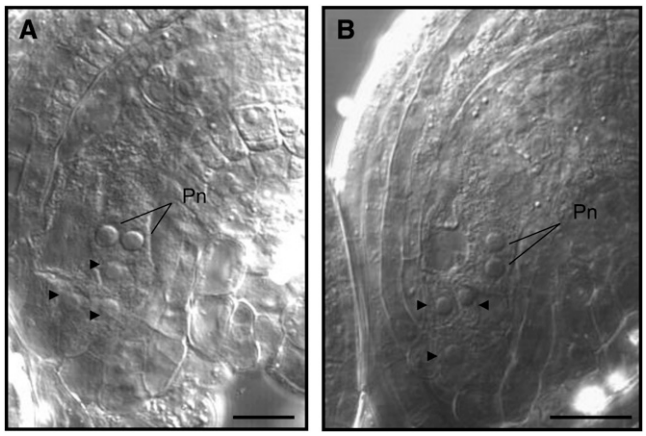

Figure 8. *oiwa* Embryo Sacs Present an Atypical Arrangement of Nuclei at the Micropylar End of the Embryo Sac.

(A) Wild-type embryo sac at FG5 stage. Two nuclei are localized at the micropylar edge of the female gametophyte, while one nucleus is located at a central position of the micropylar pole. Nuclei are indicated by arrowheads.

(B) Embryo sac from an *oiwa-1/OIWA* pistil showing abnormal positions of nuclei at the micropylar pole of the embryo sacs at FG5 stage. Nuclei are indicated by arrowheads.

Pn, polar nuclei. Bars = 25 μm.

already reported to have nuclei fusion defects (Kägi et al., 2010). To explore this possibility, we studied mitochondrial functional status using the membrane potential ($\Delta\psi$m) indicator JC-1. JC-1 is a lipophilic dye that can selectively enter into mitochondria and reversibly change color from green to red as the membrane potential increases. In healthy cells with high mitochondrial $\Delta\psi$m, JC-1 spontaneously forms complexes with intense red fluorescence. On the other hand, in mitochondria with low $\Delta\psi$m, JC-1 remains in the monomeric form, which exhibits only green fluorescence (Y. Wang et al., 2010). We examined embryo sacs at the FG6 stage from both wild-type and *oiwa-1/OIWA* pistils for JC-1 fluorescence. When wild-type pistils were examined, the embryo sacs showed a ratio of red to green fluorescence that dispersed around a mean value of 1.996 (Figures 9A, 9B, and 9E). Also, it was noticeable that mitochondria were localized predominantly around the central cell nucleus (Figure 9A). When *oiwa-1/OIWA* pistils were analyzed, mitochondria were not only localized around the central cell nucleus, but they were also detected at a high density in the egg apparatus cells. In this case, the ratio values showed a wider range of dispersion, with embryo sacs showing ratio values around 1.9 as in wild-type pistils, as well as embryo sacs with lower ratio values (Figure 9). Accordingly, the distribution pattern of JC-1 fluorescent ratio exhibited by the embryo sacs from *oiwa-1/OIWA* pistils was significantly different from the one shown by wild-type pistils (assessed by Kruskal-Wallis nonparametric one-way analysis of variance, $P < 0.001$). This result is consistent with the fact that *oiwa* mutant embryo sacs might contain dysfunctional mitochondria, possibly due to ROS-induced damage of the organelle, which in turn could explain part of the gametophytic phenotypes observed, as previously suggested. To further study mitochondria distribution along wild-type and *oiwa* embryo sacs, we used the mitochondrion-specific dye MitoTracker red. Although mitochondria could be detected along the whole embryo sac, they appeared to be more concentrated in the central cell of all embryo sacs analyzed (n = 194; see Supplemental Figure 7 online). When *oiwa-1/OIWA* pistils were analyzed, a fraction of embryo sacs showed high density of mitochondria not only in the central cell but also in the egg apparatus cells (30 out of 188), indicating that ~32% of the mutants have an unusual distribution of mitochondria in the embryo sac. To address if the differences observed were the result of cellular damage, we analyzed plasma membrane integrity in wild-type and mutant embryo sacs from emasculated flowers by staining with the lipophilic dye FM4-64 (Gordon et al., 2007; Schapire et al., 2008). FM4-64 is a dye that intercalates in the plasma membrane and fluoresces only in living cells. If the plasma membrane is damaged, massive staining is expected (Schapire et al., 2008). FM4-64 fluorescence was detected outlining cells in the majority of the mature embryo sacs present in *oiwa-1/OIWA* pistils (172 out of 186 embryo sacs analyzed 2 d after emasculation). Massive staining was only detected 4 d after emasculation in small embryo sacs, probably accounting for those that were arrested early in development (stages FG2-4; see Supplemental Figure 7 online). This result indicates that even when cells are exposed to high levels of ROS in mutant embryo sacs, the plasma membrane seems unaffected, at least in embryo sacs able to reach the FG6 to FG7 stage.

MSD1 Is Expressed in Both the Female and the Male Gametophytes of *Arabidopsis*

To study the temporal and spatial expression pattern of the *MSD1* gene during gametophytic development, the localization of *MSD1* mRNA was determined by in situ hybridization, and its expression was also analyzed in transgenic plants carrying a *promoter*:*GFP* reporter gene fusion. When we performed RNA in situ hybridization on developing ovules and anthers, *MSD1* mRNA was not detected until maturity of the gametophytes. *MSD1* mRNA was abundantly localized in the egg apparatus, principally in the synergid cells of embryo sacs at the FG6 stage (Figures 10A to 10D). *MSD1* expression was also detected in antipodal cells of the embryo sacs and in mature pollen grains (Figures 10C, 10D, 10G, and 10H). No *MSD1* mRNA was detected in the sporophytic tissues of the ovule (Figures 10A to 10D). During embryo development, *MSD1* expression was observed abundantly in the embryo proper and suspensor at least until the two-cell stage (Figures 10E and 10F).

The expression of *GFP* driven by the entire intergenic region located upstream *MSD1* translation start site (*pMSD1*:*GFP*) was also analyzed in ovules from wild-type transgenic plants. *GFP* expression was first detected during sporogenesis at the nucellus and was maintained later on inside the embryo sac during development until stage FG6, when it could be detected along the whole embryo sac. At the FG7 stage, expression was restricted to the micropylar end of the embryo sac, while expression in the central cell and at the chalazal region seemed to be downregulated (Figures 10I to 10L). During embryogenesis, GFP expression was detected both in the embryo proper and at the suspensor, at least until the one-cell stage (Figure 10M).

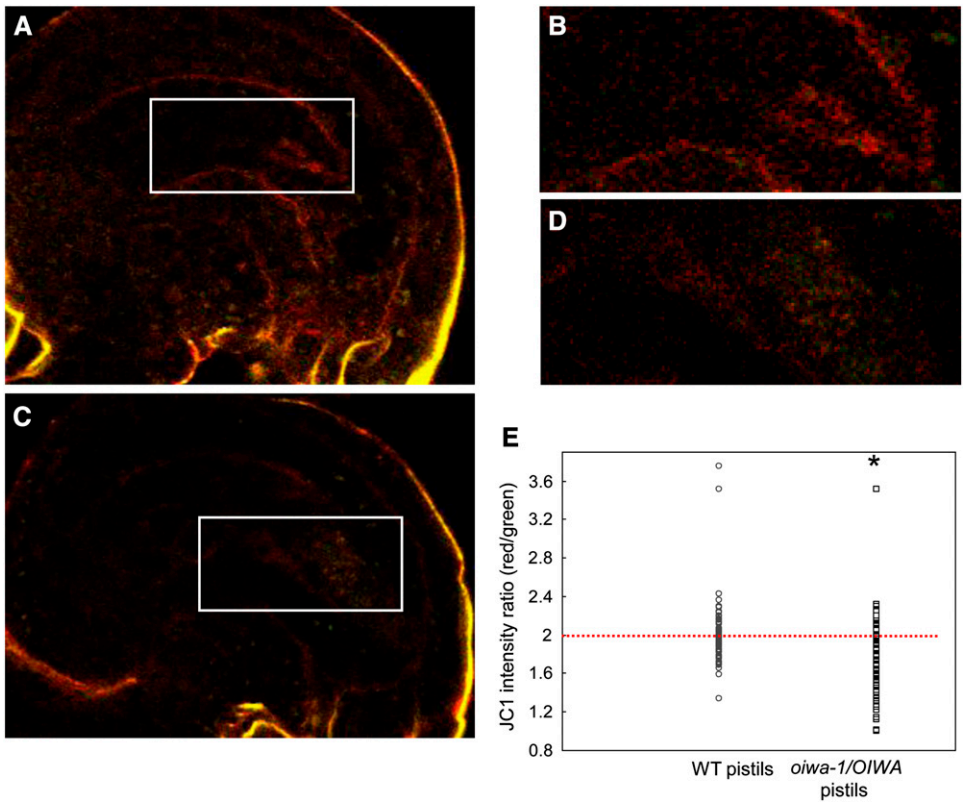

Figure 9. Mitochondrial Membrane Potential in Wild-Type and *oiwa* Embryo Sacs.

(A) Representative image showing JC-1 fluorescence in an ovule from a wild-type pistil. The red/green ratio obtained for this image in the embryo sac was 2.290. The box indicates the area of the embryo sac enlarged in **(B)**.

(B) Section of the embryo sac of the ovule pictured in **(A)** showing JC-1 staining.

(C) Representative image showing JC-1 fluorescence inside the embryo sac of an ovule from an *oiwa-1/OIWA* pistil. The red/green ratio obtained for this image in the embryo sac was 1.330. The box indicates the area of the embryo sac enlarged in **(D)**.

(D) Section of the embryo sac pictured in **(C)** showing JC-1 staining with a red/green JC-1 fluorescence ratio of 1.330.

(E) Dispersion graph showing the values of the red/green JC-1 fluorescence ratios measured in embryo sacs from wild-type (WT) pistils (open circles) and *oiwa-1/OIWA* pistils (open squares) by Image J software. The red line indicates a ratio of 1.996, which is the mean value obtained for wild-type embryo sacs.

Asterisk indicates statistical significance (*$P < 0.001$, Kruskal-Wallis). A total of 69 embryo sacs from wild-type pistils and 70 embryo sacs from *oiwa-1/OIWA* pistils were analyzed.

DISCUSSION

Oxidative Environments Seem to Be Required at Precise Locations and Developmental Stages of the Female Gametophyte: Emerging Roles for ROS as Signaling Molecules

During megagametogenesis, we were able to detect ROS only at one stage of development. A strong, localized oxidative burst was observed around the central cell nucleus at the FG6-FG7 stage, a point in development at which antipodal degeneration takes place (Figure 6). However, no ROS were detected around antipodal cells. Interestingly, the central cell has been reported to regulate antipodal cells life span (Kägi et al., 2010). By studying the mutant *fiona*, the researchers demonstrated that central cell functional mitochondria are essential for antipodal cell death, suggesting that adjacent cells might be able to regulate the fate of neighbor cells. In agreement with those previous results, the accumulation of mitochondrial ROS that we observed concentrated around the central cell nucleus at the FG7 stage may work as a signal to trigger antipodal cell death in a non-cell-autonomous way.

It is remarkable that the central cell seems to be the main source of ROS during gametogenesis. In wild-type embryo sacs, mitochondria are concentrated in the central cell (Figure 9; see Supplemental Figure 4 online; Kägi et al., 2010). This characteristic appears to be a central cell feature, as egg apparatus cells do not contain high concentrations of mitochondria in wild-type embryo sacs. Furthermore, micropylar cells do show a high number of mitochondria in the *oiwa* background, where they are able to express a central cell–specific marker. The particular location of ROS and the fact that no expression of *MSD1* was detectable in the central cell in mature embryo sacs indicate that

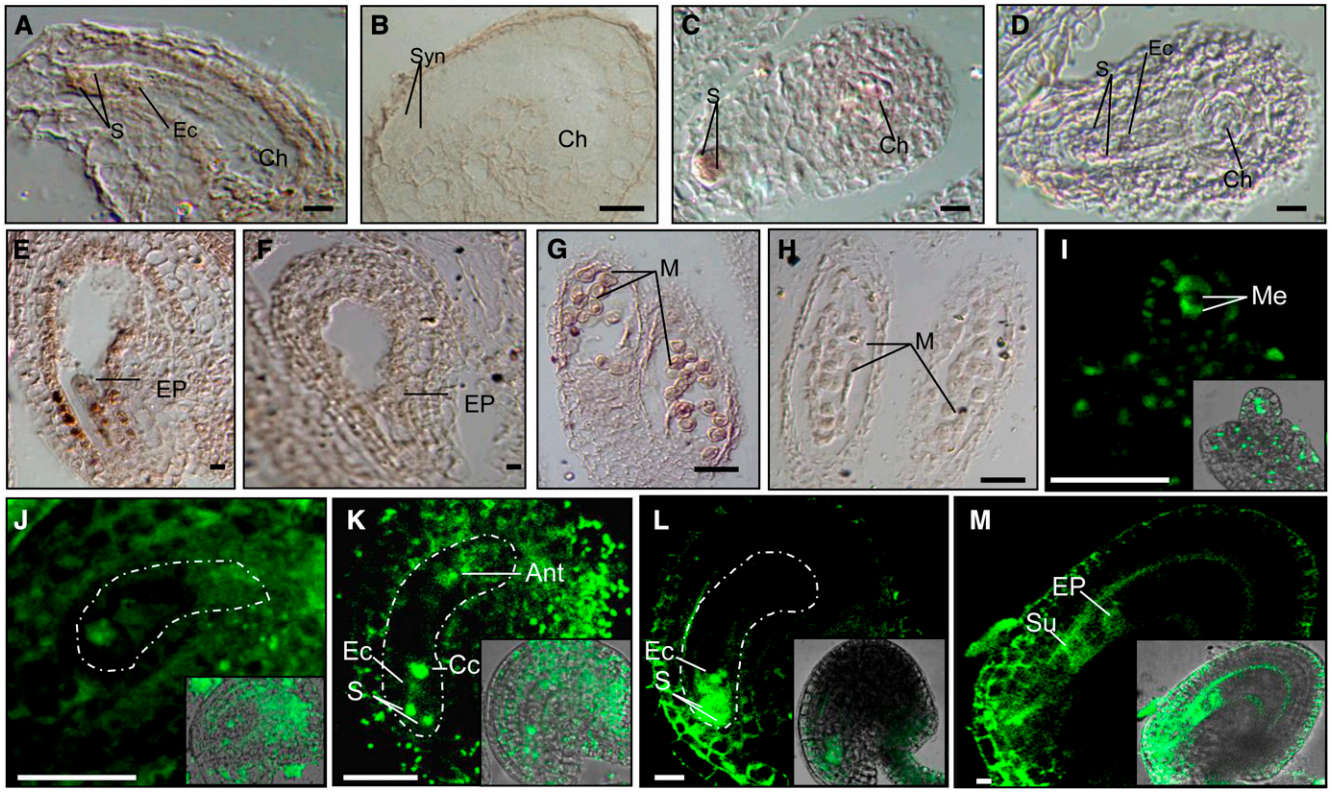

Figure 10. Temporal and Spatial Patterns of *MSD1* Expression.

(A) Localization of *MSD1* mRNA by in situ hybridization in a longitudinal section of a fully differentiated ovule.
(B) Sense probe (negative control) in a longitudinal section of a fully differentiated ovule.
(C) Localization of *MSD1* mRNA by in situ hybridization in a transversal section of a fully differentiated ovule.
(D) Sense probe (negative control) in a transversal section of a mature ovule.
(E) Localization of *MSD1* mRNA by in situ hybridization in a longitudinal section of an ovule showing a developing embryo at the one cell stage.
(F) Sense probe (negative control) in a longitudinal section of an ovule showing a developing embryo at the one cell stage.
(G) Localization of *MSD1* mRNA by in situ hybridization in longitudinal section of anthers from a flower at stage 10.
(H) Sense probe (negative control) in a longitudinal section of anthers from a flower at stage 10.
(I) Reporter gene expression in an ovule from a *pMSD1-GFP* transformant plant at megasporogenesis. The inset shows an overlay of DIC and GFP.
(J) *pMSD1-GFP* is detected inside the female gametophyte at stage FG4. Expression is also detected at the adjacent sporophytic tissues of the ovule, particularly at the chalazal end. The embryo sac is outlined in white. The inset shows an overlay of DIC and GFP.
(K) At stage FG5, GFP is detected along the whole embryo sac and associated with nuclei. GFP is also detected at the chalazal end of the ovule. The embryo sac is outlined in white. The inset shows an overlay of DIC and GFP.
(L) At FG6-7 stage, GFP is restricted to the micropylar cells of the embryo sac: synergid cells and egg cell. The embryo sac is outlined in white. The inset shows an overlay of DIC and GFP.
(M) After fertilization, the reporter gene expression is detected both at the suspensor and in the embryo proper of a developing embryo at one cell stage. The inset shows an overlay of DIC and GFP.
Ant, antipodal cells; Cc, central cell; Ch, chalaza; Ec, egg cell; EP, embryo proper; M, microspores; Me, megaspores; S, synergid cells; Su, suspensor. Bars = 25 μm.

central cell mitochondria are able to maintain high levels of ROS without undergoing structural or functional damage. Similar features are common in mammalian cells such as macrophages, which are able to maintain high levels of ROS during inflammatory responses (Forman and Torres, 2001). These results lead to the following question: What are the consequences of this localized oxidative burst? The central cell plays critical roles during female gametophyte development, affecting antipodal cell degeneration (Kägi et al., 2010), pollen tube guidance (Chen et al., 2007), and the initiation of endosperm after fertilization (Curtis and Grossniklaus, 2008). Furthermore, the central cell has been recently reported to be the source of 24-nucleotide small interference RNAs, which silence transposons in plants. These large small interference RNA populations arise through activation of DEMETER and inactivation of the DNA methyltransferase MET1 in the central cell and are proposed to migrate to the egg cell where they guide de novo DNA methylation (Ibarra et al., 2012; Wöhrmann et al., 2012). Thus, the central cell oxidative status might be important not only for regulating developmental aspects of the gametophyte, such as antipodal cell

death and fertilization, but also for influencing the DNA methylation process, as has been reported for other systems (Lim et al., 2008; Hitchler and Domann, 2009).

Interestingly, ROS accumulation was also observed in one of the synergid cells of mature embryo sacs after manual pollination of the pistils. This oxidative burst seems to respond to an increase in cytosolic peroxide and not to mitochondrial superoxide, a result that is in concordance with the high levels of *MSD1* expression observed in the egg apparatus (Figures 7 and 10). Our findings suggest that this ROS accumulation depends on pistil pollination, as we were not able to detect it in ovules from emasculated pistils. However, it precedes pollen tube contact, as it was observed at a time point at which we did not detect pollen tubes reaching embryo sacs (5 HAP). This result indicates that embryo sacs prepare for pollen tube arrival by sensing a long-distance signal. This long-distance signal could be generated either by the pollen–pistil interaction or by growing pollen tubes and is perceived by the female gametophytes inside the ovules. Embryo sacs respond by creating an oxidative environment that might be required for pollen tube reception. In agreement with this idea, mutations in *FERONIA* (*FER*), a receptor-like kinase that was shown to activate ROS production in root hairs, impair pollen tube rupture in embryo sacs (Escobar-Restrepo et al., 2007; Duan et al., 2010; Kanaoka and Torii, 2010). A similar response to pollination was reported for the *AMC* gene, encoding a peroxin required for protein import into peroxisomes and essential for pollen tube discharge, whose expression is induced by pollen deposition on the pistils (Boisson-Dernier et al., 2008). In root hairs, FER is a cell surface receptor, acting upstream of the Rho-related small GTPase ROP. FER interacts with ROP and is predicted to promote both auxin- and ROS-mediated growth. A pathway involving FER, ROPGEFs, and RAC/ROPs regulates NADPH oxidase-dependent ROS production in root hairs. Subsequently, ROS stimulate Ca^{2+} channels to increase the cytoplasmic calcium concentration, which promotes root hair tip growth (Duan et al., 2010). A similar pathway may be activated in the female gametophyte in response to pollination. FER-dependent ROS production in synergid cells might be required for pollen tube growth arrest or burst. Also, cytoplasmic Ca^{2+} oscillation in synergid cells upon pollen tube arrival have recently been described (Iwano et al., 2012). Cytoplasmic Ca^{2+} increases after contact with the pollen tube and reaches a maximum at pollen tube rupture. The role of these oscillations is still unclear, but the increase in Ca^{2+} concentration may be involved in the induction of the programmed cell death that follows pollen tube burst in the receptive synergid. Likewise, pathogen-associated Ca^{2+} elevation in plant cells activates a signal transduction pathway that leads to the hypersensitive response and cell death (Ma and Berkowitz, 2007).

Upon pollen tube arrival, different ROS contribute to the oxidative status of synergid cells. Both mitochondrial and cytosolic superoxides are detected in the synergid cells, and peroxide is also detected by DAB. As a high oxidative status might be required for fertilization success, this result explains why the high levels of ROS present in *oiwa* embryo sacs did not interfere with pollen tube attraction and fertilization of the mutant embryo sacs that reached maturity (Figure 4). However, embryo development is arrested very early in mutant embryo sacs, indicating that regulation of ROS levels from the maternal side is essential for proper embryo development. Accordingly, ROS are excluded from the embryo sac after fertilization and *MSD1* expression is upregulated during early embryogenesis (Figure 10).

MSD1 Regulates ROS Homeostasis during Female Gametogenesis and Is Essential for Normal Development, Patterning, and Fertilization

MSD1 may function by confining ROS at precise temporal and spatial domains during embryo sac development. In agreement with this idea, *MSD1* expression was detected during megasporogenesis, where only peroxide but not mitochondrial superoxide was detected. Also, *MSD1* expression is tightly regulated during megagametogenesis. Its expression was detected along the whole embryo sac early in development. As gametogenesis progresses, *MSD1* expression becomes restricted to the egg apparatus cells, and it is not detectable in the central cell by in situ hybridization or by promoter-GFP fusion studies. Concordantly, ROS show a complementary pattern, as they cannot be detected in the egg apparatus but are detectable in the central cell. These results are in agreement with a role for MSD1 in regulating oxidative domains along the embryo sac, and they explain why the central cell seems to be the principal source of ROS in the mature female gametophyte.

oiwa embryo sacs showed high levels of ROS from stage FG5 onward. These high levels were not restricted to the central cell but were also detectable in the micropylar cells of the embryo sac (Figure 6; see Supplemental Figure 4 online). Furthermore, we observed that not only did mitochondrial superoxide accumulate in the mutant gametophytes, but cytosolic peroxide levels also increased. This peroxide accumulation outside the mitochondria may have been the result of superoxide dismutation after escaping the mitochondria through mitochondrial permeability transition pores or voltage-dependent anion channels, as was demonstrated for other systems (Han et al., 2003; Tran et al., 2012). However, as cytosolic superoxide levels are also increased in mutant embryo sacs, we cannot discount that other sources of ROS, such as NAPH oxidase activity, are also involved in the increase of ROS levels detected in these gametophytes, probably as a consequence of mitochondrial dysfunction. Thus, MSD1 seems to be required not only to regulate mitochondrial ROS levels but also to regulate cellular ROS homeostasis along the whole embryo sac during development.

Interestingly, central cell identity is no longer restricted to the large central cell in *oiwa* female gametophytes. The expression of two specific central cell markers, DD65 and *pMEA*:*NLS*:*GUS*, is also detected in micropylar cells of the mutant embryo sacs, indicating that MSD1 is necessary for restricting central cell fate. As high levels of ROS are observed from developmental stage FG5 in mutant embryo sacs and thus preceding gametophytic cell specification, it is possible that ROS might function in determining central cell features.

oiwa gametophytes showed additional defects during development, ranging from embryo sacs showing mitotic arrest to gametophytes with problems in polar nuclei fusion or with aberrant egg apparatus. These differences probably arise from variable expressivity of the mutation in the female gametophyte,

a phenomenon that is not uncommon, which has been reported for other mutants affected in female gametophyte development (Kirioukhova et al., 2011; Sørmo et al., 2011). A fraction of *oiwa* embryo sacs showed mitotic arrest. This defect may be due to the fact that intracellular ROS oscillations might regulate key components of the cell division machinery. ROS were reported to regulate Ca^{2+}gradients and to participate in the regulation of proteins such as cyclin-dependent kinases, mitogen-activated proteins, and possibly aurora kinases and therefore to regulate cell cycle progression, microtubule organization, and cell plate formation (Livanos et al., 2012a, 2012b). The abnormal nuclei migration patterns observed in some *oiwa* embryo sacs may also account for the elevated concentration of ROS in mutant gametophytes, as ROS might also disturb microtubule organization or dynamics. The formation of atypical tubulin paracrystals has been reported to occur under elevated ROS levels via mitogen-activated protein kinase activation and MAP65 phosphorylation (Livanos et al., 2012b).

As aerobic organisms, plants live in an oxygen-rich environment. ROS and their chemical reactions are part of their basic metabolism. Traditionally considered to be deleterious molecules, ROS are currently emerging as essential signaling molecules modulating different cellular and intracellular pathways involved in normal growth and development in many different organisms. Plants, animals, and even fungi have evolved mechanisms in which potentially harmful ROS are used as messengers to fulfill an extensive range of key biological processes (Malagnac et al., 2004; Wu et al., 2005; Gapper and Dolan, 2006; Owusu-Ansah and Banerjee, 2009). This work shows that ROS are not only involved in the development of plant sporophytic tissues but also in female gametogenesis and fertilization. Although further work is required to deeply understand the molecular basis of ROS signaling during plant sexual reproduction, MSD1 seems to be essential for precisely regulating their levels both spatially and temporally during female gametogenesis.

METHODS

Plant Materials and Growth Conditions

Mn-SOD mutant SALK_122275 (*oiwa-1*) and GK-847D04-025833 (*oiwa-2*) *Arabidopsis thaliana* lines were obtained from the ABRC (Ohio State University) (Alonso et al., 2003). Both lines were backcrossed twice to wild-type Columbia prior to their use. SALK_122275 presented two T-DNA insertions: one in chromosome 4 (at the intergenic region between At4g11030 and At4g11040 genes) and one in chromosome 3 (on At3g10920). The single insertion in At3g10920 after backcrosses and all genotypes were confirmed by PCR-based genotyping.

Marker lines ET1119 and ET884 were a gift from Ueli Grossniklaus' lab and were analyzed as previously described (Pagnussat et al., 2007). Antipodal marker pAt1g36340:GUS was generated at Venkatesan Sundaresan's lab and analyzed as described (Yu et al., 2005). Central cell marker DD65 was a gift from Gary Drews' lab and was analyzed as described (Steffen et al., 2007; Leshem et al., 2012). The central cell marker line pMEA:NLS:GUS was a gift from Rita Groß-Hardt's lab and was analyzed as previously described (Pagnussat et al., 2007).Wild-type plants used were *Arabidopsis thaliana* var Col-0.

When indicated, seeds were sterilized in 20% (v/v) sodium hypochlorite, washed with sterile water, and plated on Murashige and Skoog plates with 50 μg/mL kanamycin and/or 15 μg/mL sulfadiazine. Resistant (green) seedlings were then transferred onto soil and grown under the conditions described above.

Molecular Characterization of Insertional Lines

Genotyping of the T-DNA insertion lines used in this study was performed as previously described (Pagnussat et al., 2007). For *oiwa-1*, the left border–genomic sequence junction was determined by PCR in plants showing kanamycin resistance using the T-DNA–specific primer LBb1 (5′-GCGTGGACCGCTTGCTGCAACT-3′) combined with the genomic sequence-specific primers *oiwa-1* RP (5′-TGATCTCAAGACCCAGCAAAC-3′) and LP (5′-CGATCCTCCTTCATTTCTTCC-3′). For *oiwa-2*, the left border–genomic sequence junction was determined by PCR in plants showing sulfadiazine resistance using the T-DNA–specific primer LBb1 combined with the genomic sequence specific primer *oiwa-2* RP (5′-ACAATGGTTTGTGAAAGCAGC-3′) and LP (5′-GAGCTCAAGAAGCAACAATCC-3′).

Segregation Analysis

For self-cross analysis, heterozygous plants were allowed to self-pollinate and progeny seed was collected. The F1 seed was germinated on selective growth medium containing 50 mg/mL kanamycin (*oiwa-1*) or 15 mg/mL of sulfadizine (*oiwa-2*), and the numbers of resistant and sensitive plants were scored. Reciprocal crosses were performed as described previously (Pagnussat et al., 2005).

Constructions

Genomic DNA was extracted from rosette leaves as described (Capron et al., 2008). The *pMSD1*:*GFP* transcriptional fusion was generated as follows: The putative *MSD1* promoter region was amplified by PCR using the following combination of primers: forward (5′-CATCGGAGAATTAAAAAAAAAAAACCG-3′) and reverse (5′-TGTTGGAATGAAGATTTGTTTGTCC-3′). The amplicon was cloned into *pENTR/TOPO* (Invitrogen) and the sequence was verified. The resultant plasmid *pENTR-pMSD1* was subjected to the LR reaction using the destination vector pMDC107 (Curtis and Grossniklaus, 2003).

Transformation of *Agrobacterium tumefaciens* and *Arabidopsis*

Vectors were introduced into *Agrobacterium* strain GV3101 by electroporation. Transformation into *Arabidopsis* plants was performed by the floral dip method (Clough and Bent, 1998). Transformants were selected based on their ability to survive on Murashige and Skoog medium with 15 mg L^{-1} hygromycin. Resistant (green seedlings with true leaves) were then transferred to soil and grown under the conditions described above.

Morphological and Histological Analyses

Flowers from different developmental stages with at least 40 ovules per pistil were dissected and cleared overnight in Hoyer's solution. For GUS staining, developing carpels and siliques were dissected and incubated in GUS staining buffer as previously described (Pagnussat et al., 2007). Ovules were observed under a Nikon Eclipse Ti microscope using differential interference contrast (DIC) optics. Images were captured with a DS-Fi1 camera (Nikon) using the NIS-Element F 3.0 program. For pollen tube staining, pistils were manually pollinated, softened with 5 M NaOH at 65°C for 5 min, washed with tap water, and treated with 0.1% aniline blue in 0.1 M K_3PO_4 buffer, pH 8.3, for 3 h. After incubation, pistils were washed with 0.1 M K_3PO_4 buffer, mounted on a microscope slide, and carefully squashed under a cover slip. The pistils were observed using a fluorescence microscope (Nikon Eclipse Ti microscope).

Mitochondria distribution was analyzed using MitoTracker red (Molecular probes). Stock solutions (1 mM in DMSO) were prepared fresh for each use. The stock solution was diluted in buffer PBS, pH 7.2, at 10 μM for each experiment (working solution). Pistils were dissected on a microscopic slide and incubated in the working solution for 30 min at room temperature in complete darkness. After incubation, pistils were immediately observed using confocal microscopy (Nikon Eclipse C1 Plus confocal microscope) using EZ-C1 3.80 imaging software and Ti-Control.

Plasma membrane integrity was analyzed using FM4-64 (Molecular Probes) as described (Schapire et al., 2008). Briefly, pistils were incubated in a 50 μM FM4-64 solution for 45 min and mounted on a microscopic slide. After incubation, pistils were immediately observed using confocal microscopy (Nikon Eclipse C1 Plus confocal microscope) using EZ-C1 3.80 imaging software and Ti-Control.

ROS Detection and Image Analysis

H_2DCFDA was prepared as a 10 mM stock solution in DMSO and frozen at −20°C. MitoSOX red was prepared fresh at a 5 mM concentrated solution in DMSO for each use. The stock solutions were diluted in 20 mM HEPES buffer, pH 7.2 (buffer A), at 1:1000 in each experiment. Pistils were dissected in buffer A on a microscopic slide and incubated for 30 min at room temperature in working solution containing the dyes. After incubation, pistils were washed with buffer A and immediately observed using confocal microscopy (Nikon Eclipse C1 Plus confocal microscope) using EZ-C1 3.80 imaging software and Ti-Control. H_2DCFDA was excited by the 488-nm line of the laser, and images were acquired with the green photomultiplier channel of the confocal microscope. For MitoSOX red, the 408-nm line of the confocal laser was used for excitation (Robinson et al., 2006), and the red photomultiplier channel of the confocal microscope was used for image acquisition.

In situ superoxide was detected using the NBT staining method. Pistils were vacuum-infiltrated (two cycles of 5 min) in a 10 mM sodium phosphate buffer, pH 7.8, containing 10 mM NaN3 and 0.1% NBT (Promega) and incubated in complete darkness for 30 min at 37°C. Pistils were dissected under a dissecting microscope, and the ovules were cleared overnight in Hoyer's solution.

In situ H_2O_2 was observed by DAB staining. Pistils were vacuum-infiltrated (three cycles of 5 min) with a DAB solution (1 mg·mL^{-1}, pH 3.8). After incubation at room temperature in total darkness, samples were dissected and cleared overnight in Hoyer's solution. H_2O_2 was visualized as a brown color at the site of DAB polymerization. NBT- and DAB-stained samples were observed under a Zeiss Axioplan Imager.A2 microscope under DIC optics. Images were captured with an Axiocam HRC charge-coupled device camera (Zeiss) using the Axiovision program (version 3.1).

Studies of Mitochondrial Membrane Potential ($\Delta\Psi$m)

JC-1 was purchased from Molecular Probes. Pistils were dissected and incubated in 10 μg/mL JC-1 for 30 min at room temperature. After incubation, pistils were washed with buffer A, and images were collected using a confocal microscope (Nikon Eclipse C1 Plus). The intensities of green (excitation/emission wavelength = 485/538 nm) and red (excitation/emission wavelength = 485/590 nm) fluorescence were analyzed for 69 individual embryo sacs from wild-type plants and for 70 individual embryo sacs from mutant plants. Images were analyzed using Image J software (NIH). The ratio of red to green fluorescence of JC-1 images was calculated using NIH Image J software (http://rsb.info.nih.gov/ij/). The outline of each embryo sac was circled using the freehand tool to create a region of interest and was saved using the multimeasure tool. The average intensity per area was analyzed in both the red and green channels. Then, the ratio was obtained for each region for all regions of interest.

In Situ Hybridization

In situ hybridization was performed as described previously (Vielle-Calzada et al., 1999). An antisense probe was synthesized from a ZeroBlunt TOPO vector (Invitrogen) containing a 171-bp *MSD1* cDNA fragment that was amplified using the following combination of primers: forward (5′-CCATTCGATTTTCTGGAAGAACCTT-3′) and reverse (5′-CCGAGC-CACACCCATCCAGCC-3′). Sense and antisense *MSD1* probes were transcribed in vitro with SP6 and T7 RNA polymerase (Promega), respectively. Pistils and inflorescences were fixed with 4% formaldehyde, dehydrated through a conventional ethanol series, and embedded in Paraplast (Sigma-Aldrich). Sections (10- to 15-μm thick) were made with a HYDRAX M15 microtome (Zeiss) and dewaxed with xylene. In situ hybridization and signal detection were performed according to previous reports (Vielle-Calzada et al., 1999). The images were obtained with a Nikon Eclipse Ti microscope using DIC optics. Images were captured with a DS-Fi1 camera (Nikon) using the NIS-Element F 3.0 program.

Fluorescence Microscopy and Image Analysis

Pistils were dissected in 10 mM phosphate buffer on a microscopic slide and immediately observed under a fluorescence microscope. Fluorescence detection was done using confocal microscopy (Nikon Eclipse C1 Plus confocal microscope) using EZ-C1 3.80 imaging software and Ti-Control.

Statistical Analysis

The Kruskal-Wallis test on ranks was performed for non-normal populations using the SIGMASTAT 3.1 statistical tool (Sigma-Aldrich).

Bioinformatics and Phylogenetic Analysis

Amino acid sequences of related proteins used here were obtained from GenBank (National Center for Biotechnology Information). The amino acid sequences were aligned using MEGA (version 5.05) and the following parameters: for pairwise alignment, a gap opening penalty of 10 and gap extension penalty of 0.1; gap opening penalty and gap extension penalty for multiple alignment, 10 and 0.2, respectively; Gonnet protein weight matrix; residue-specific penalties, ON; hydrophilic penalties, ON; gap separation distance, 4; end gap separation, OFF; use negative matrix, OFF; and delay divergent cutoff, 30% (Tamura et al., 2011). Graphic display of identities was visualized using Geneious Basic 5.6.3 (http://www.geneious.com) based on identity matrix (Drummond et al., 2012).

A phylogenetic tree was constructed using the neighbor-joining method and the default settings of MEGA (version 5.05) (Saitou and Nei, 1987; Tamura et al., 2011). The optimal tree (sum of branch length = 0.82304186) is shown in Figure 1. The percentages of replicate trees in which the associated taxa clustered together in the bootstrap test (1000 replicates) are shown on the branches (Felsenstein, 1985). The evolutionary distances were computed using the Poisson correction method and are in the units of the number of amino acid substitutions per site (Zuckerkandl and Pauling, 1965). The analysis involved eight amino acid sequences. All ambiguous positions were removed for each sequence pair. There were a total of 240 positions in the final dataset.

Accession Numbers

Sequence data from this article can be found in the Arabidopsis Genome Initiative under the following accession numbers: At3g10920 (*MSD1*, Mn-SOD), At4g11030 (AMP-dependent synthetase and ligase family protein), and At4g11040 (protein phosphatase 2C family protein). The National Center for Biotechnology Information accession numbers for Mn-SOD proteins discussed in this article and the supporting information are *Arabidopsis* AEE74977, *Brassica napus* ACA50527, sunflower (*Helianthus*

annuus) ABH11433, cotton (*Gossypium hirsutum*) ABA00455, *Zantedeschia aethiopica* AAC63379, wheat (*Triticum aestivum*) AAB68035, maize (*Zea mays*) AAA33512, and rice (*Oryza sativa*) AAA62657.

Supplemental Data

The following materials are available in the online version of this article.

Supplemental Figure 1. Scheme Showing the Developmental Stages during Wild-Type Female Gametophyte Development in *Arabidopsis thaliana*.

Supplemental Figure 2. Female Gametogenesis Is Impaired in *oiwa-2* Mutants.

Supplemental Figure 3. Normal Differentiation of Antipodal Cells in *oiwa-1* Embryo Sacs.

Supplemental Figure 4. ROS Detection in Wild-Type and *oiwa* Embryo Sacs.

Supplemental Figure 5. Pollen Tube Growth in Wild-Type Pistils.

Supplemental Figure 6. Expression of the Synthetic Reporter *DR5*:*GFP* in Embryo Sacs.

Supplemental Figure 7. Localization of Mitochondria and Membrane Integrity in Wild-Type and Mutant *Arabidopsis* Embryo Sacs.

Supplemental Table 1. Analysis of the Ovules Present in Wild-Type and *oiwa*/*OIWA* Pistils 2 d after Emasculation.

Supplemental Table 2. Analysis of the Ovules Present in Wild-Type and *oiwa*/*OIWA* Pistils 2 d after Pollination with Wild-Type Pollen.

ACKNOWLEDGMENTS

M.V.M. is a postdoctoral fellow of Consejo Nacional de Investigaciones Científicas y Técnicas (CONICET). D.F.F., E.J.Z., and G.C.P. are CONICET researchers. This research was funded by Agencia Nacional de Promoción Científica y Técnica, CONICET, and the Howard Hughes Medical Institute. We thank Rita Groß-Hardt for marker line *pMEA*:*NLS*:*GUS*, Ueli Grossniklaus for marker lines ET1119 and ET884 seeds, and Gary Drews for DD65 seeds. We thank members of the mitochondrial biology lab for helpful discussions and suggestions. We thank Claudia Casalongue, Ayelen Distefano, and Lorenzo Lamattina for critical reading of the article and Daniela Villamonte for technical assistance.

AUTHOR CONTRIBUTIONS

G.C.P, M.V.M., and E.J.Z. designed the research. M.V.M. and G.C.P. performed research experiments. D.F.F. performed bioinformatics analysis. G.C.P. and D.F.F. analyzed data. V.S. designed the mutant screening. G.C.P., E.J.Z., and M.V.M. wrote the article.

Received January 7, 2013; revised March 22, 2013; accepted April 25, 2013; published May 7, 2013.

REFERENCES

Alonso, J.M., et al. (2003). Genome-wide insertional mutagenesis of *Arabidopsis thaliana*. Science **301:** 653–657.

Alscher, R.G., Erturk, N., and Heath, L.S. (2002). Role of superoxide dismutases (SODs) in controlling oxidative stress in plants. J. Exp. Bot. **53:** 1331–1341.

Fehér, A., Otvös, K., Pasternak, T.P., and Szandtner, A.P. (2008). The involvement of reactive oxygen species (ROS) in the cell cycle activation (G(0)-to-G(1) transition) of plant cells. Plant Signal. Behav. **3:** 823–826.

Bi, Y., Chen, W., Zhang, W., Zhou, Q., Yun, L., and Xing, D. (2012). Production of reactive oxygen species, impairment of photosynthetic function and dynamic changes in mitochondria are early events in cadmium-induced cell death in *Arabidopsis thaliana*. Biol. Cell **101:** 629–643.

Boisson-Dernier, A., Frietsch, S., Kim, T.H., Dizon, M.B., and Schroeder, J.I. (2008). The peroxin loss-of-function mutation abstinence by mutual consent disrupts male-female gametophyte recognition. Curr. Biol. **18:** 63–68.

Bowler, C., Van Camp, W., Van Montagu, M., and Inzé, D. (1994). Superoxide dismutase in plants. Crit. Rev. Plant Sci. **13:** 199–218.

Capron, A., Gourgues, M., Neiva, L.S., Faure, J.E., Berger, F., Pagnussat, G., Krishnan, A., Alvarez-Mejia, C., Vielle-Calzada, J.P., Lee, Y.R., Liu, B., and Sundaresan, V. (2008). Maternal control of male-gamete delivery in *Arabidopsis* involves a putative GPI-anchored protein encoded by the LORELEI gene. Plant Cell **20:** 3038–3049.

Carol, R.J., and Dolan, L. (2006). The role of reactive oxygen species in cell growth: Lessons from root hairs. J. Exp. Bot. **57:** 1829–1834.

Chen, Y.-H., Li, H.-J., Shi, D.-Q., Yuan, L., Liu, J., Sreenivasan, R., Baskar, R., Grossniklaus, U., and Yang, W.-C. (2007). The central cell plays a critical role in pollen tube guidance in *Arabidopsis*. Plant Cell **19:** 3563–3577.

Christensen, C.A., King, E.J., Jordan, J.R., and Drews, G.N. (1997). Megagametogenesis in *Arabidopsis* wild type and the Gf mutant. Sex. Plant Reprod. **10:** 49–64.

Christensen, C.A., Subramanian, S., and Drews, G.N. (1998). Identification of gametophytic mutations affecting female gametophyte development in *Arabidopsis*. Dev. Biol. **202:** 136–151.

Clough, S.J., and Bent, A.F. (1998). Floral dip: A simplified method for Agrobacterium-mediated transformation of *Arabidopsis thaliana*. Plant J. **16:** 735–743.

Curtis, M.D., and Grossniklaus, U. (2003). A gateway cloning vector set for high-throughput functional analysis of genes in planta. Plant Physiol. **133:** 462–469.

Curtis, M.D., and Grossniklaus, U. (2008). Molecular control of autonomous embryo and endosperm development. Sex. Plant Reprod. **21:** 79–88.

De Tullio, M.C., Jiang, K., and Feldman, L.J. (2010). Redox regulation of root apical meristem organization: Connecting root development to its environment. Plant Physiol. Biochem. **48:** 328–336.

Duan, Q., Kita, D., Li, C., Cheung, A.Y., and Wu, H.-M. (2010). FERONIA receptor-like kinase regulates RHO GTPase signaling of root hair development. Proc. Natl. Acad. Sci. USA **107:** 17821–17826.

Escobar-Restrepo, J.M., Huck, N., Kessler, S., Gagliardini, V., Gheyselinck, J., Yang, W.C., and Grossniklaus, U. (2007). The FERONIA receptor-like kinase mediates male-female interactions during pollen tube reception. Science **317:** 656–660.

Evans, M.M.S. (2007). The indeterminate gametophyte1 gene of maize encodes a LOB domain protein required for embryo Sac and leaf development. Plant Cell **19:** 46–62.

Felsenstein, J. (1985). Confidence limits on phylogenies: An approach using the bootstrap. Evolution **39:** 783–791.

Foreman, J., Demidchik, V., Bothwell, J.H.F., Mylona, P., Miedema, H., Torres, M.A., Linstead, P., Costa, S., Brownlee, C., Jones, J.D.G., Davies, J.M., and Dolan, L. (2003). Reactive oxygen species produced by NADPH oxidase regulate plant cell growth. Nature **422:** 442–446.

Forman, H.J., and Torres, M. (2001). Redox signaling in macrophages. Mol. Aspects Med. **22:** 189–216.

Gapper, C., and Dolan, L. (2006). Control of plant development by reactive oxygen species. Plant Physiol. **141:** 341–345.

Gazarian, I.G., Lagrimini, L.M., Mellon, F.A., Naldrett, M.J., Ashby, G.A., and Thorneley, R.N. (1998). Identification of skatolyl hydroperoxide and its role in the peroxidase-catalysed oxidation of indol-3-yl acetic acid. Biochem. J. **333:** 223–232.

Gordon, S.P., Heisler, M.G., Reddy, G.V., Ohno, C., Das, P., and Meyerowitz, E.M. (2007). Pattern formation during de novo assembly of the *Arabidopsis* shoot meristem. Development **134:** 3539–3548.

Gross-Hardt, R., Kägi, C., Baumann, N., Moore, J.M., Baskar, R., Gagliano, W.B., Jürgens, G., and Grossniklaus, U. (2007). LACHESIS restricts gametic cell fate in the female gametophyte of *Arabidopsis*. PLoS Biol. **5:** e47.

Grunewald, W., and Friml, J. (2010). The march of the PINs: Developmental plasticity by dynamic polar targeting in plant cells. EMBO J. **29:** 2700–2714.

Han, D., Antunes, F., Canali, R., Rettori, D., and Cadenas, E. (2003). Voltage-dependent anion channels control the release of the superoxide anion from mitochondria to cytosol. J. Biol. Chem. **278:** 5557–5563.

Hitchler, M.J., and Domann, F.E. (2009). Metabolic defects provide a spark for the epigenetic switch in cancer. Free Radic. Biol. Med. **47:** 115–127.

Ibarra, C.A., et al. (2012). Active DNA demethylation in plant companion cells reinforces transposon methylation in gametes. Science **337:** 1360–1364.

Iwano, M., Ngo, Q.A., Entani, T., Shiba, H., Nagai, T., Miyawaki, A., Isogai, A., Grossniklaus, U., and Takayama, S. (2012). Cytoplasmic Ca^{2+} changes dynamically during the interaction of the pollen tube with synergid cells. Development **139:** 4202–4209.

Jansen, M.A.K., van den Noort, R.E., Tan, M.Y., Prinsen, E.L., Lagrimini, L.M., and Thorneley, R.N.F. (2001). Phenol-oxidizing peroxidases contribute to the protection of plants from ultraviolet radiation stress. Plant Physiol. **126:** 1012–1023.

Joo, J.H., Bae, Y.S., and Lee, J.S. (2001). Role of auxin-induced reactive oxygen species in root gravitropism. Plant Physiol. **126:** 1055–1060.

Kägi, C., Baumann, N., Nielsen, N., Stierhof, Y.-D., and Gross-Hardt, R. (2010). The gametic central cell of *Arabidopsis* determines the lifespan of adjacent accessory cells. Proc. Natl. Acad. Sci. USA **107:** 22350–22355.

Kanaoka, M.M., and Torii, K.U. (2010). FERONIA as an upstream receptor kinase for polar cell growth in plants. Proc. Natl. Acad. Sci. USA **107:** 17461–17462.

Kaye, Y., Golani, Y., Singer, Y., Leshem, Y., Cohen, G., Ercetin, M., Gillaspy, G., and Levine, A. (2011). Inositol polyphosphate 5-phosphatase7 regulates the production of reactive oxygen species and salt tolerance in *Arabidopsis*. Plant Physiol. **157:** 229–241.

Kirioukhova, O., Johnston, A.J., Kleen, D., Kägi, C., Baskar, R., Moore, J.M., Bäumlein, H., Gross-Hardt, R., and Grossniklaus, U. (2011). Female gametophytic cell specification and seed development require the function of the putative *Arabidopsis* INCENP ortholog WYRD. Development **138:** 3409–3420.

Kliebenstein, D.J., Monde, R.-A., and Last, R.L. (1998). Superoxide dismutase in *Arabidopsis*: an eclectic enzyme family with disparate regulation and protein localization. Plant Physiol. **118:** 637–650.

Lee, Y., Kim, M., and Kim, S. (2007). Cell type identity in *Arabidopsis* roots is altered by both ascorbic acid-induced changes in the redox environment and the resultant endogenous auxin response. J. Plant Biol. **50:** 484–489.

Leshem, Y., Johnson, C., Wuest, S.E., Song, X., Ngo, Q.A., Grossniklaus, U., and Sundaresan, V. (2012). Molecular characterization of the glauce mutant: A central cell-specific function is required for double fertilization in *Arabidopsis*. Plant Cell **24:** 3264–3277.

Lim, S.-O., Gu, J.-M., Kim, M.S., Kim, H.-S., Park, Y.N., Park, C.K., Cho, J.W., Park, Y.M., and Jung, G. (2008). Epigenetic changes induced by reactive oxygen species in hepatocellular carcinoma: Methylation of the E-cadherin promoter. Gastroenterology **135:** 2128–2140.

Livanos, P., Apostolakos, P., and Galatis, B. (2012a). Plant cell division: ROS homeostasis is required. Plant Signal. Behav. **7:** 771–778.

Livanos, P., Galatis, B., Quader, H., and Apostolakos, P. (2012b). Disturbance of reactive oxygen species homeostasis induces atypical tubulin polymer formation and affects mitosis in root-tip cells of *Triticum turgidum* and *Arabidopsis thaliana*. Cytoskeleton (Hoboken) **69:** 1–21.

Ma, W., and Berkowitz, G.A. (2007). The grateful dead: Calcium and cell death in plant innate immunity. Cell. Microbiol. **9:** 2571–2585.

Malagnac, F., Lalucque, H., Lepère, G., and Silar, P. (2004). Two NADPH oxidase isoforms are required for sexual reproduction and ascospore germination in the filamentous fungus *Podospora anserina*. Fungal Genet. Biol. **41:** 982–997.

Miller, G., Shulaev, V., and Mittler, R. (2008). Reactive oxygen signaling and abiotic stress. Physiol. Plant. **133:** 481–489.

Mittler, R., Vanderauwera, S., Gollery, M., and Van Breusegem, F. (2004). Reactive oxygen gene network of plants. Trends Plant Sci. **9:** 490–498.

Morgan, M.J., Lehmann, M., Schwarzländer, M., Baxter, C.J., Sienkiewicz-Porzucek, A., Williams, T.C., Schauer, N., Fernie, A.R., Fricker, M.D., Ratcliffe, R.G., Sweetlove, L.J., and Finkemeier, I. (2008). Decrease in manganese superoxide dismutase leads to reduced root growth and affects tricarboxylic acid cycle flux and mitochondrial redox homeostasis. Plant Physiol. **147:** 101–114.

Myhre, O., Andersen, J.M., Aarnes, H., and Fonnum, F. (2003). Evaluation of the probes 2′,7′-dichlorofluorescin diacetate, luminol, and lucigenin as indicators of reactive species formation. Biochem. Pharmacol. **65:** 1575–1582.

Okuda, S., et al. (2009). Defensin-like polypeptide LUREs are pollen tube attractants secreted from synergid cells. Nature **458:** 357–361.

Owusu-Ansah, E., and Banerjee, U. (2009). Reactive oxygen species prime Drosophila haematopoietic progenitors for differentiation. Nature **461:** 537–541.

Pagnussat, G.C., Alandete-Saez, M., Bowman, J.L., and Sundaresan, V. (2009). Auxin-dependent patterning and gamete specification in the *Arabidopsis* female gametophyte. Science **324:** 1684–1689.

Pagnussat, G.C., Yu, H.J., Ngo, Q.A., Rajani, S., Mayalagu, S., Johnson, C.S., Capron, A., Xie, L.F., Ye, D., and Sundaresan, V. (2005). Genetic and molecular identification of genes required for female gametophyte development and function in *Arabidopsis*. Development **132:** 603–614.

Pagnussat, G.C., Yu, H.J., and Sundaresan, V. (2007). Cell-fate switch of synergid to egg cell in *Arabidopsis* eostre mutant embryo sacs arises from misexpression of the BEL1-like homeodomain gene BLH1. Plant Cell **19:** 3578–3592.

Perl-Treves, R., and Galun, E. (1991). The tomato Cu,Zn superoxide dismutase genes are developmentally regulated and respond to light and stress. Plant Mol. Biol. **17:** 745–760.

Robinson, K.M., Janes, M.S., Pehar, M., Monette, J.S., Ross, M.F., Hagen, T.M., Murphy, M.P., and Beckman, J.S. (2006). Selective fluorescent imaging of superoxide in vivo using ethidium-based probes. Proc. Natl. Acad. Sci. USA **103:** 15038–15043.

Rodríguez, A.A., Grunberg, K.A., and Taleisnik, E.L. (2002). Reactive oxygen species in the elongation zone of maize leaves are necessary for leaf extension. Plant Physiol. **129:** 1627–1632.

Royall, J.A., and Ischiropoulos, H. (1993). Evaluation of 2′,7′-dichlorofluorescin and dihydrorhodamine 123 as fluorescent probes for intracellular H2O2 in cultured endothelial cells. Arch. Biochem. Biophys. **302:** 348–355.

Saitou, N., and Nei, M. (1987). The neighbor-joining method: A new method for reconstructing phylogenetic trees. Mol. Biol. Evol. **4:** 406–425.

Samis, K., Bowley, S., and McKersie, B. (2002). Pyramiding Mn-superoxide dismutase transgenes to improve persistence and biomass production in alfalfa. J. Exp. Bot. **53:** 1343–1350.

Sandaklie-Nikolova, L., Palanivelu, R., King, E.J., Copenhaver, G. P., and Drews, G.N. (2007). Synergid cell death in *Arabidopsis* is triggered following direct interaction with the pollen tube. Plant Physiol. **144:** 1753–1762.

Schapire, A.L., Voigt, B., Jasik, J., Rosado, A., Lopez-Cobollo, R., Menzel, D., Salinas, J., Mancuso, S., Valpuesta, V., Baluska, F., and Botella, M.A. (2008). *Arabidopsis* synaptotagmin 1 is required for the maintenance of plasma membrane integrity and cell viability. Plant Cell **20:** 3374–3388.

Sørmo, C.G., Brembu, T., Winge, P., and Bones, A.M. (2011). *Arabidopsis thaliana* MIRO1 and MIRO2 GTPases are unequally redundant in pollen tube growth and fusion of polar nuclei during female gametogenesis. PLoS ONE **6:** e18530.

Srilunchang, K.O., Krohn, N.G., and Dresselhaus, T. (2010). DiSUMO-like DSUL is required for nuclei positioning, cell specification and viability during female gametophyte maturation in maize. Development **137:** 333–345.

Steffen, J.G., Kang, I.H., Macfarlane, J., and Drews, G.N. (2007). Identification of genes expressed in the *Arabidopsis* female gametophyte. Plant J. **51:** 281–292.

Tamura, K., Peterson, D., Peterson, N., Stecher, G., Nei, M., and Kumar, S. (2011). MEGA5: Molecular evolutionary genetics analysis using maximum likelihood, evolutionary distance, and maximum parsimony methods. Mol. Biol. Evol. **28:** 2731–2739.

Tran, T.P., Tu, H., Liu, J., Muelleman, R.L., and Li, Y.-L. (2012). Mitochondria-derived superoxide links to tourniquet-induced apoptosis in mouse skeletal muscle. PLoS ONE **7:** e43410.

Tsukagoshi, H., Busch, W., and Benfey, P.N. (2010). Transcriptional regulation of ROS controls transition from proliferation to differentiation in the root. Cell **143:** 606–616.

Ulmasov, T., Murfett, J., Hagen, G., and Guilfoyle, T.J. (1997). Aux/IAA proteins repress expression of reporter genes containing natural and highly active synthetic auxin response elements. Plant Cell **9:** 1963–1971.

Van Breusegem, F., and Dat, J.F. (2006). Reactive oxygen species in plant cell death. Plant Physiol. **141:** 384–390.

Van Breusegem, F., Slooten, L., Stassart, J.-M., Botterman, J., Moens, T., Van Montagu, M., and Inze, D. (1999). Effects of overproduction of tobacco MnSOD in maize chloroplasts on foliar tolerance to cold and oxidative stress. J. Exp. Bot. **50:** 71–78.

Vielle-Calzada, J.P., Thomas, J., Spillane, C., Coluccio, A., Hoeppner, M.A., and Grossniklaus, U. (1999). Maintenance of genomic imprinting at the *Arabidopsis* medea locus requires zygotic DDM1 activity. Genes Dev. **13:** 2971–2982.

Wang, Y., Ying, Y., Chen, J., and Wang, X. (2004). Transgenic *Arabidopsis* overexpressing Mn-SOD enhanced salt-tolerance. Plant Sci. **167:** 671–677.

Wang, Y., Zhu, Y., Ling, Y., Zhang, H., Liu, P., Baluska, F., Samaj, J., Lin, J., and Wang, Q. (2010). Disruption of actin filaments induces mitochondrial Ca2+ release to the cytoplasm and [Ca2+]c changes in *Arabidopsis* root hairs. BMC Plant Biol. **10:** 53.

Wang, Y.C., Qu, G.Z., Li, H.Y., Wu, Y.J., Wang, C., Liu, G.F., and Yang, C.P. (2010). Enhanced salt tolerance of transgenic poplar plants expressing a manganese superoxide dismutase from *Tamarix androssowii*. Mol. Biol. Rep. **37:** 1119–1124.

Wöhrmann, H.J.P., Gagliardini, V., Raissig, M.T., Wehrle, W., Arand, J., Schmidt, A., Tierling, S., Page, D.R., Schöb, H., Walter, J., and Grossniklaus, U. (2012). Identification of a DNA methylation-independent imprinting control region at the *Arabidopsis* MEDEA locus. Genes Dev. **26:** 1837–1850.

Wu, R.F., Xu, Y.C., Ma, Z., Nwariaku, F.E., and Sarosi, G.A., Jr., andTerada, L.S. (2005). Subcellular targeting of oxidants during endothelial cell migration. J. Cell Biol. **171:** 893–904.

Xu, J., Zhang, H.Y., Xie, C.H., Xue, H.W., Dijkhuis, P., and Liu, C.M. (2005). EMBRYONIC FACTOR 1 encodes an AMP deaminase and is essential for the zygote to embryo transition in *Arabidopsis*. Plant J. **42:** 743–756.

Yu, H.J., Hogan, P., and Sundaresan, V. (2005). Analysis of the female gametophyte transcriptome of *Arabidopsis* by comparative expression profiling. Plant Physiol. **139:** 1853–1869.

Zhang, L., Li, Y., Xing, D., and Gao, C. (2009). Characterization of mitochondrial dynamics and subcellular localization of ROS reveal that HsfA2 alleviates oxidative damage caused by heat stress in *Arabidopsis*. J. Exp. Bot. **60:** 2073–2091.

Zuckerkandl, E., and Pauling, L. (1965). Evolutionary Divergence and Convergence in Proteins. (New York: Academic Press).